AD NUMBER

AD850098

NEW LIMITATION CHANGE

TO

Approved for public release, distribution unlimited

FROM

Distribution authorized to U.S. Gov't. agencies and their contractors; Critical Technology; FEB 1969. Other requests shall be referred to Army Research Office, Attn: CRD-AA-IP, Durham, NC 27706.

AUTHORITY

usaro itrm 12 aug 1971

UTC 2296-FR

MEASUREMENT OF PARTICLE DRAG COEFFICIENTS IN FLOW REGIMES ENCOUNTERED BY PARTICLES IN A ROCKET NOZZLE

AD850098

FINAL TECHNICAL REPORT
FOR THE PERIOD 1 SEPTEMBER 1967
THROUGH 28 FEBRUARY 1969

by

C.T. Crowe, W.R. Babcock, P.G. Willoughby, R.L. Carlson

Prepared for
Department of the Army
U.S. Army Research Office
Durham, North Carolina

Contract No. DAH-C04-67-C-0057

This document is subject to special export controls, and each transmittal to foreign governments or foreign nationals may be made only with prior approval of U.S. Army Research Office. attn: CRD-AA-IP, Durham, North Carolina 27706

The findings in this report are not to be construed as an official Department of the Army position unless so designated by other authorized documents.

United Technology Center DIVISION OF UNITED AIRCRAFT CORPORATION
SUNNYVALE, CALIFORNIA

56

UTC 2296-FR

MEASUREMENT OF PARTICLE DRAG COEFFICIENTS IN FLOW REGIMES ENCOUNTERED BY PARTICLES IN A ROCKET NOZZLE

FINAL TECHNICAL REPORT
FOR THE PERIOD 1 SEPTEMBER 1967 THROUGH 28 FEBRUARY 1969

by

C. T. Crowe, W. R. Babcock, P. G. Willoughby, R. L. Carlson

Prepared for
Department of the Army
U.S. Army Research Office
Durham, North Carolina

Contract No. DAH-C04-67-C-0057
Project 6656-E

United Technology Center DIVISION OF UNITED AIRCRAFT CORPORATION
SUNNYVALE, CALIFORNIA

AD 850098

United Technology Center DIVISION OF UNITED AIRCRAFT CORPORATION

21 April 1969

ERRATUM

UTC 2296-FR

MEASUREMENT OF PARTICLE DRAG COEFFICIENTS IN FLOW REGIMES ENCOUNTERED BY PARTICLES IN A ROCKET NOZZLE

Final Technical Report for the Period
1 September 1967 through 28 February 1969

Contract No. DAH-C04-67-C-0057

Report mailed 9 April 1969

The exponent 0.7 fell out from the Knudsen number (Kn) in an expression occurring in equation 39 (page 40) and in the lower center of figure 17 (page 41). Please add the exponent in these two places. The expression will then correctly read:

$$- - - \exp\left[- Kn^{0.7} \, e^{Kn} - - - \right.$$

C T C / C..

C. T. Crowe
Project Scientist

USAF ZERO DEFECTS

SUNNYVALE, CALIFORNIA 94088 Phone 739-4880

ABSTRACT

Under contract to the Army Research Office, United Technology Center has conducted an experimental investigation to determine the drag coefficient of particles in flow regimes encountered in a rocket nozzle. The acquisition of these data leads to more reliable predictions of nozzle performance inefficiencies owing to gas-particle flow.

The Mach number-Reynolds number regime traversed by a particle in a rocket nozzle is described. The experiment to determine drag coefficient data in this flow regime consists of the electrostatic acceleration of micron-size particles to sonic velocities and detection of their velocity decay in a chamber conditioned to provide the desired flow parameters. The operation of the experiment, method of data reduction, and analysis of the experimental error are presented.

The data are reduced in terms of a nondimensional drag coefficient and are correlated with comparable data obtained in other flow regimes. An empirical relation is generated for the drag coefficient as a function of Reynolds and Knudsen numbers. This relation is recommended for use in calculations of gas-particle flow in rocket nozzles.

CONTENTS

ILLUSTRATIONS

TABLES

SYMBOLS

Latin

a	speed of sound
A	representative area
C_D	drag coefficient
$\overline{C}_D$	nondimensional drag coefficient
$C_{D_{inc}}$	drag coefficient for incompressible flow
C_{D_I}	"inviscid" drag coefficient
$C_{D_{FM}}$	free-molecule-flow drag coefficient
d_c	distance between Faraday cages
d_r	total range distance
E_s	signal voltage
F_D	drag force
i	current
Kn	Knudsen number
N	number of measurement stations in tracking section
N_v	number of measurement stations in velocity-measuring section
m	particle mass
M	Mach number
P	pressure
Q	statistical factor
q	particle charge
r_p	particle radius
R	resistance
Re	Reynolds number
S	speed ratio
s	distance traveled by particle
T_g	gas temperature
T_p	particle temperature
t	time
t_o	zero reference time
u_f	particle velocity in velocity-measuring section
u_g	gas velocity
u_o	initial particle velocity
u_p	particle velocity
V	accelerating potential

Greek

α	constant related to drag coefficient
γ	ratio of specific heats
η	variable
μ_g	gas viscosity
σ^2	variance
ρ_g	gas density
ρ_p	particle density
λ	mean free path

BLANK PAGE

1.0 INTRODUCTION

The use of a metallic fuel, such as aluminum, in rocket propellants augments the available energy per unit mass and improves performance. The improvement is not as large as thermodynamic calculations indicate because the micron size particles of metal oxide produced upon combustion of the metal and carried out by the exhaust gases are unable to maintain kinetic and thermal equilibrium with the exhaust gases; this results in a performance inefficiency. Analyses of gas-particle flow in rocket nozzles have been developed to predict this inefficiency[(1)*] but fundamental data for the aerodynamic drag force on the particles have not been available. The aim of this project was the experimental determination of this aerodynamic force in flow regimes encountered in a rocket nozzle.

The nondimensional parameter which characterizes the aerodynamic drag force on a particle in a gas stream is the drag coefficient, C_D, defined as

$$C_D = \frac{F_D}{\frac{1}{2}\rho_g (u_g - u_p)^2 A} \qquad (1)$$

where F_D is the drag force, ρ_g the gas density, u_g the gas velocity, u_p the particle velocity, and A a representative particle area. In general, the drag coefficient of an object is dependent on several parameters such as shape and orientation with respect to the flow, M, Re, and turbulence level. Experiments[(1)] have shown that particles found in rocket nozzles are spherical in shape, and order-of-magnitude analyses indicate that the particle drag coefficient is primarily a function of M and Re.

The M-Re regime traversed by a particle in a typical rocket nozzle is illustrated in figure 1. A complete gamut of flow regimes from continuum to free-molecule flow are encountered as the particle moves from the rocket chamber, through the throat, and into the expansion section. No data exist for the drag coefficient of a sphere in the flow regimes bounded by Re less than 1,000 and M less than 2. A reasonable formula for the drag coefficient in this

*Parenthetical superscript numbers denote references appearing on page 46.

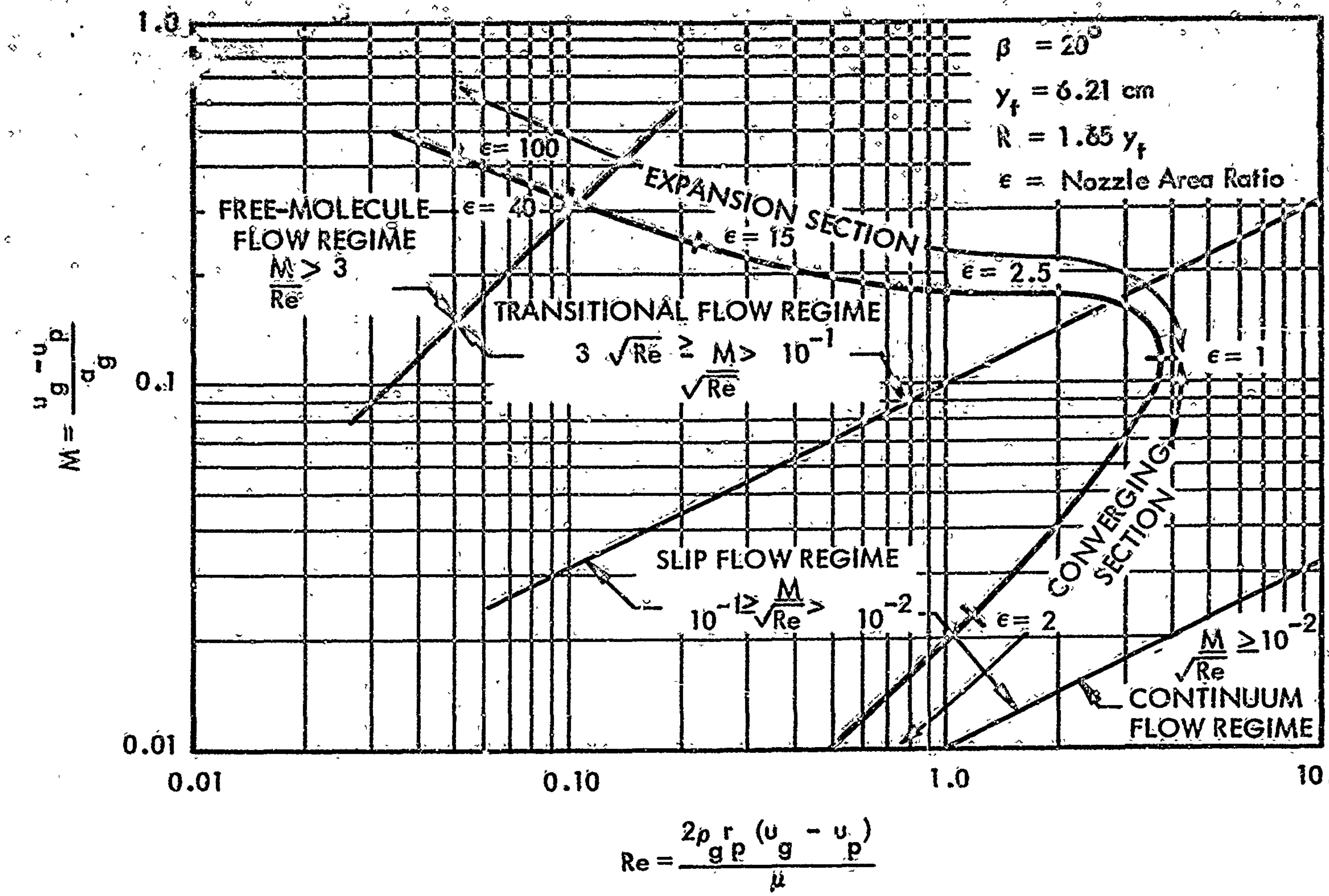

Figure 1. Flow Regimes Traversed by a Particle in a Rocket Nozzle

90560

region has been devised[2] but its validity is questionable until confirmed by experimental data.

The following sections describe the development and operation of an experiment to obtain the desired drag coefficient data. The results are discussed and an empirical equation representing the data is presented.

2.0 DESIGN AND DEVELOPMENT OF THE EXPERIMENTAL TECHNIQUE

There are two primary methods by which the drag coefficient of an object can be measured; one is to suspend the object in a gas stream (e.g., in a wind tunnel) and measure the drag force directly, and the other is to fire the object in a ballistic range and deduce the drag coefficient from time-distance data. The major difficulty in using the wind-tunnel technique to obtain data in the flow regime of interest lies in the requirement for accurate measurement of very small forces. The design complexities of a large, low-density wind tunnel and suspension system, together with extremely sensitive force-measuring instrumentation, suggest the impracticality of the wind-tunnel technique for this study.

The small drag forces that are characteristic of the M-Re regime of interest also preclude the use of a conventional ballistic range. The difficulty lies in the prohibitively long distances that a reasonably sized projectile would travel before a detectable change in velocity occurs. Employing Stokes' drag law to provide indicative results and suggest the significant parameters, yields

$$S = \frac{2}{9} u_o \frac{\rho_p r_p^2}{\mu_g} \left(1 - \frac{u_p}{u_o}\right) \tag{2}$$

where S is the distance traveled by a spherical projectile with radius r_p before its velocity has decayed to u_p. The projectile's initial velocity is u_o, and ρ_p the projectile's density, and μ_g the gas viscosity. The equation indicates that a 1-mm projectile with a density of 3 gm/cc and fired in air at 300 m/sec will travel 250 m before a 10% velocity decay ensues. The above equation suggests, however, that the ballistic range method is effective if very small projectiles can be accelerated to a sufficiently large velocity and if their time histories during deceleration can be recorded accurately. The calculations show that the projectiles must be between 1 micron and 50 microns in diameter and must achieve velocities up to 300 m/sec to provide data in the flow regime of interest.

Acceleration of micron-sized particles to high velocities has been accomplished in experimental investigations[3,4] of meteoric impact. Briefly, the technique consisted of charging particles by subjecting them to a large potential gradient while in contact with a conducting surface, and then accelerating these charged particles through a large potential difference. Assuming charge-to-mass ratios typical of these experiments, calculations show that a potential difference of 100 kv is sufficient for drag-coefficient experiments. The size of the particles impacting on a metal sample was determined by measuring the charge and velocity of the accelerated particles and using the work-energy equality

$$qV = \frac{1}{2} m u_f^2 \qquad (3)$$

where q is the particle charge, V the accelerating potential, m the particle's mass, and u_f the final particle velocity. The velocity and charge were measured using Faraday cages which are small tubes through which the particles pass and on which they induce their charge. The Faraday cages were connected to the grid of a cathode-follower circuit and the particle passage was detected as a voltage signal on an oscilloscope. This scheme was directly adaptable to measuring particle size in the present study.

A schematic diagram of the experimental apparatus is given in figure 2. The acceleration section, differential pumping sections, and tracking section were connected by 400-micron orifices through which the particle passed as it proceeded from the acceleration to the tracking section. The acceleration section was connected to a diffusion pump, while mechanical pumps were sufficient for the differential pumping sections.

In order to produce the range of Re desired, the pressure in the tracking section ranged between 1 and 100 torr. The acceleration section, however, was maintained at 10^{-4} torr for maximum electrical insulation.(5) Feasibility calculations indicated that this pressure differential could be maintained by using two differential pumping chambers and orifices smaller than 500 microns in diameter between the four chambers. The differential pumping chamber adjacent to the acceleration chamber served as the space where the charge and velocity of the particle were measured in order to determine its size.

It was initially postulated that a Faraday cage tracking technique would be ineffective in the tracking section because the particles would rapidly lose their charge in the higher pressure environment. Thus, it was initially decided to use a tracking scheme in which the particles traversing a laser beam would reflect light onto a photomultiplier tube. However, a pilot experiment performed early in the program demonstrated that a charged particle at atmospheric conditions would not lose its charge fast enough to make the Faraday cage technique ineffective. It was also decided to use a series of

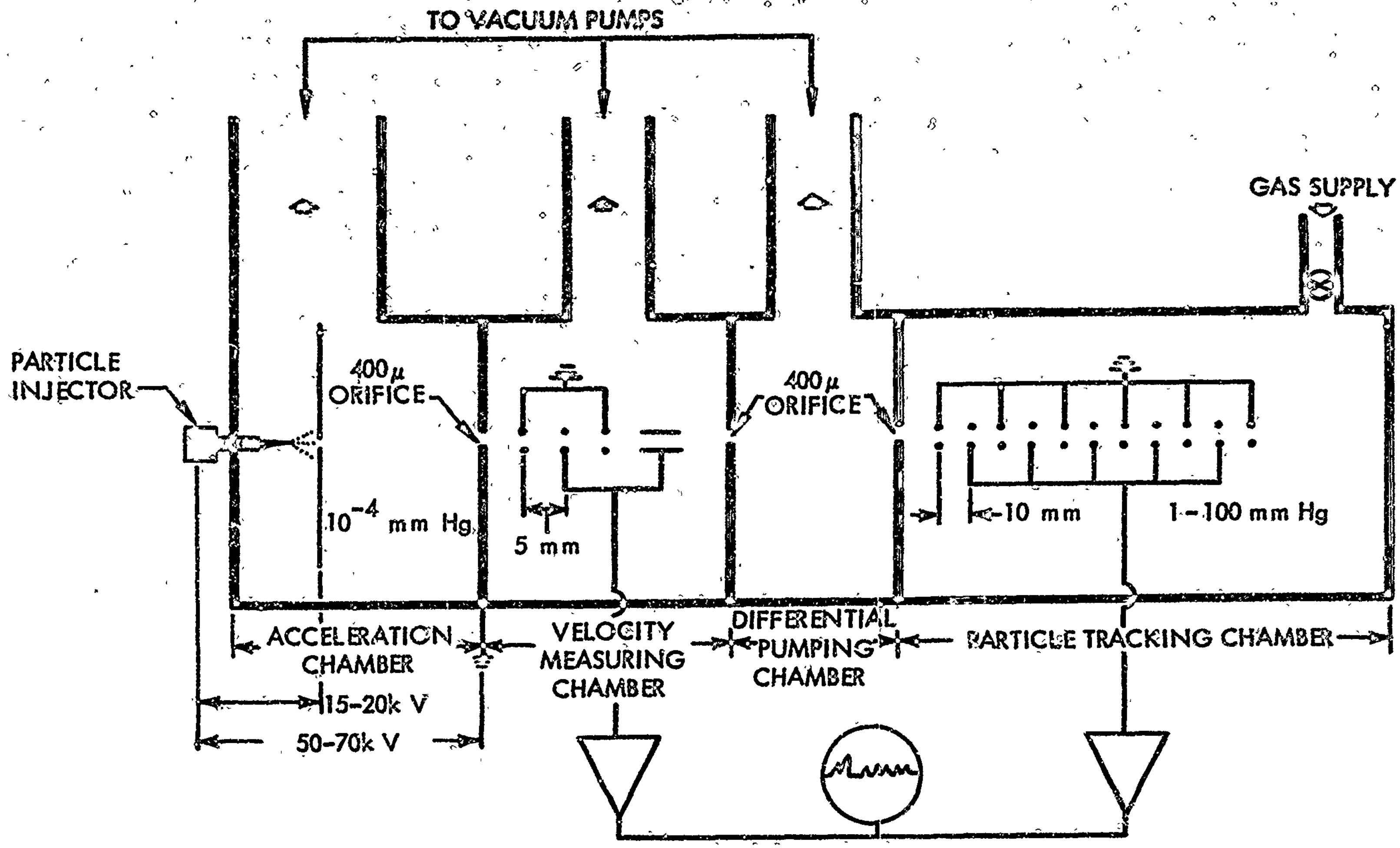

Figure 2. Schematic Diagram of Experimental Apparatus

20551

Faraday cages to measure the particle's time history in the tracking section, in lieu of the more complex optical technique. The details of each section of the apparatus are described below.

2.1 ACCELERATION CHAMBER

A diagram indicating the essential components of the acceleration chamber is shown in figure 3. A magnetized needle was mounted on a micrometer drive directly above a small hole (~80 microns in diameter) in a thin diaphragm. Magnetic particles aligned themselves in strings along the magnetic lines of force from the needle. A potential difference of from 15 to 20 kv was maintained between the needle and the diaphragm. As the needle was advanced toward the hole by the micrometer drive, the electrostatic forces overcame the magnetic ones, and one charged particle was removed from the extremity of the particle string. The charged particle proceeded through the hole and into the lower part of the chamber where it was accelerated through an additional 30 to 60 kv. A sharp conical section was used for the ground electrode to aid in alignment of the particle trajectory by causing the electrical lines of force to converge toward the cone. It was found that the sharp-edged cone was not sufficient to align the particle trajectory; probably local charge accumulations on the plexiglass walls of the container disturbed the electric field symmetry and caused trajectory misalignment. The problem was overcome by locating a copper cylinder in the chamber coaxial with the centerline of the system, which ensured a uniform charge distribution.

Carbonyl-iron particles forming strings on the tip of a magnetized needle are shown in figure 4. Generally, only one particle at a time was removed by electrostatic forces. When the supply of particles on the needle became depleted, the needle was withdrawn into the particle reservoir and acquired a new supply.

The acceleration chamber mounted in place can be seen in figure 5. It was fabricated of plexiglass to ensure sufficient electrical insulation of the high voltages. The copper cylinder inserted to make the electric field symmetric is visible. The chamber was connected to an oil diffusion pump through an angle valve and liquid-nitrogen baffle. Design calculations using the manufacturer's specifications for the speed of the diffusion pump and conductance of the baffle predicted that a pressure of 10^{-4} torr could be maintained in the acceleration chamber. However, under actual operation no pressure lower than 10^{-3} torr was achievable. At this pressure no serious electrical discharge problems were encountered at voltages up to 70 kv.

The acceleration chamber was designed for easy removal of the top to facilitate cleaning. The removed top is shown in figure 6. The plate which

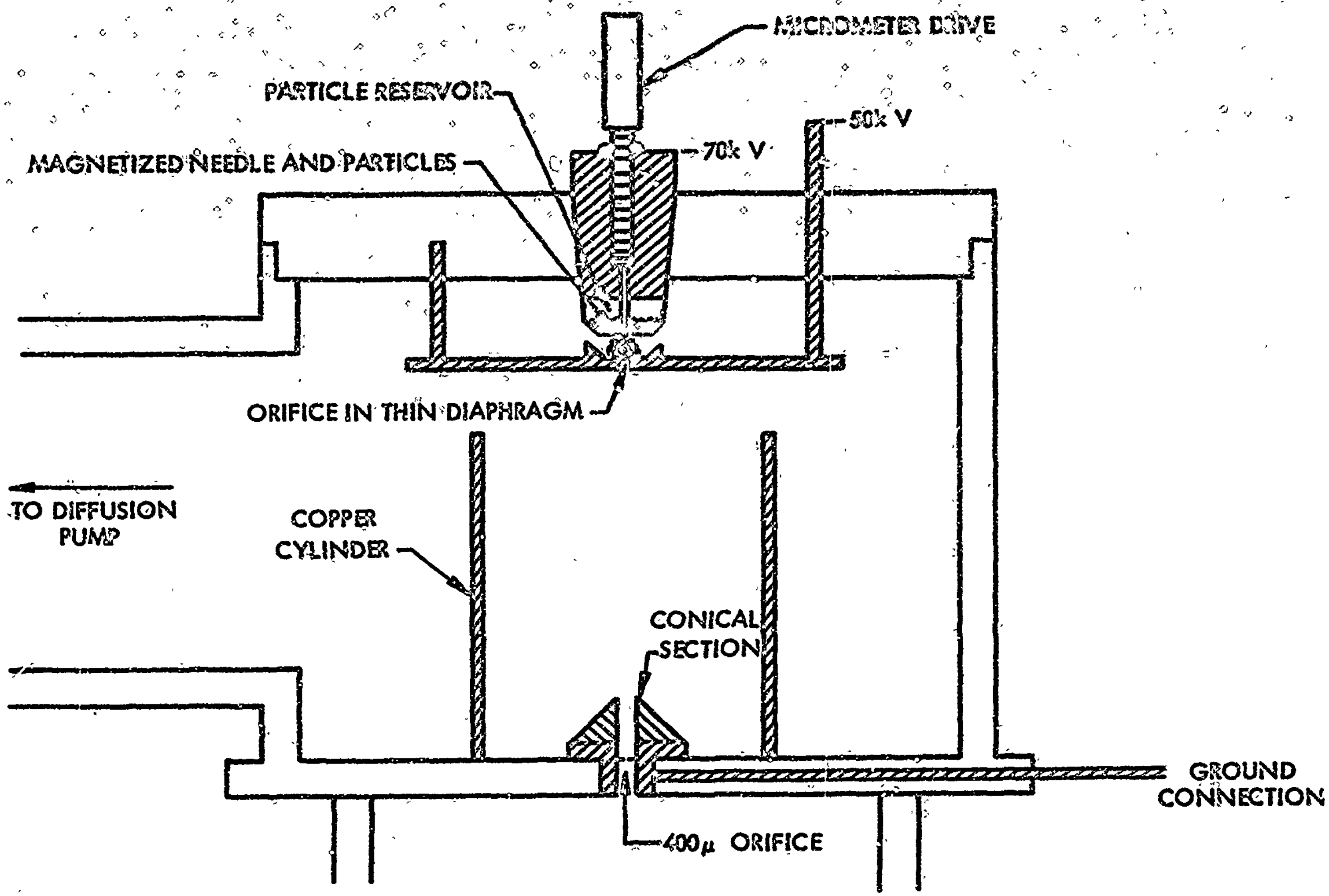

Figure 3. Schematic Diagram of Acceleration Section

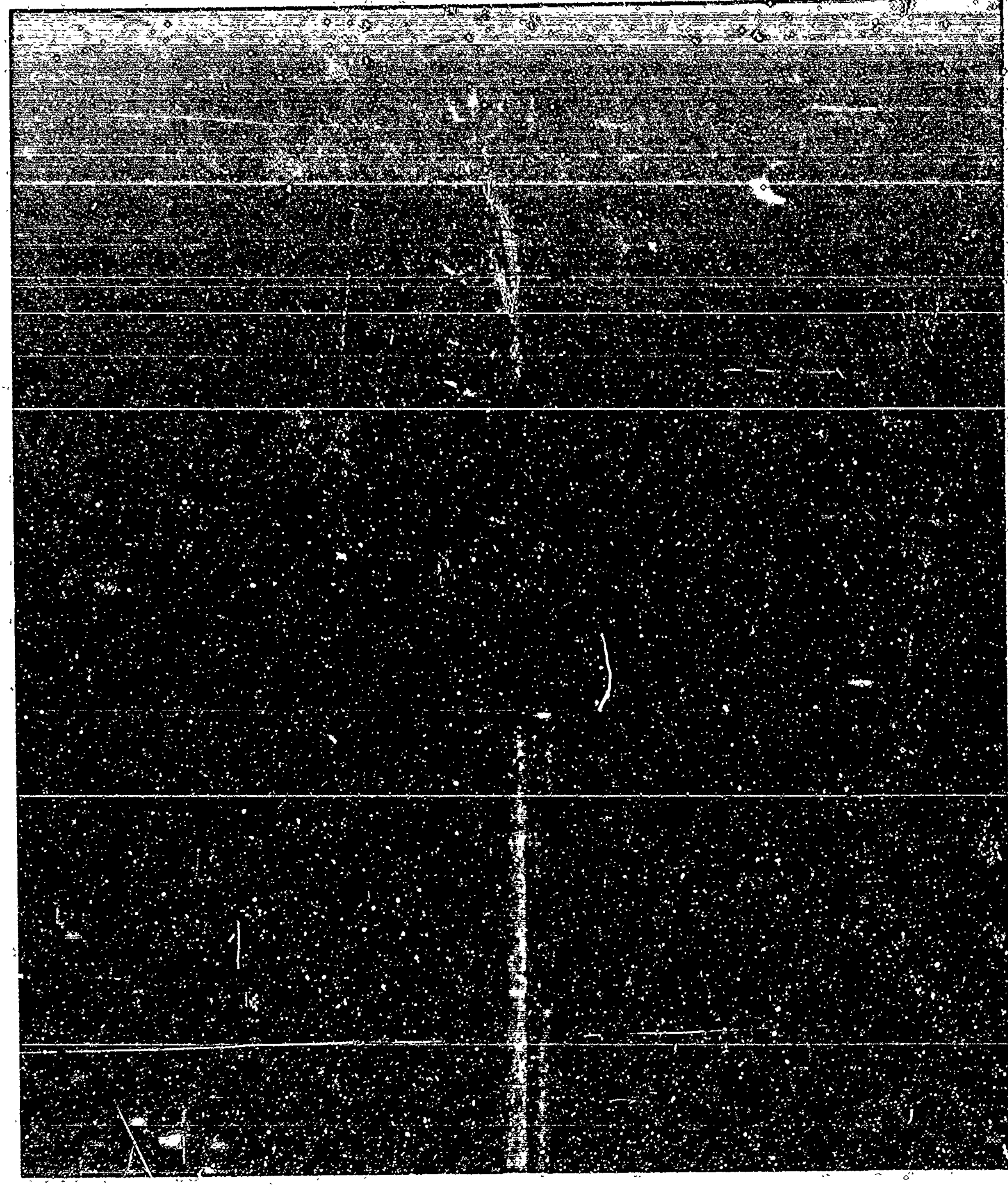

Figure 4. Electron-Microscope Photograph of Carbonyl-Iron Particles on the Tip of a Magnetized Needle 90563

Figure 5. Experimental Apparatus

90534

Figure 6. Removable Top of the Acceleration Chamber

supported the thin diaphragm with the hole beneath the needle was suspended from the plexiglass top by three metal bolts, one of which projected above the surface to provide an electrical contact to the plate and diaphragm. The insert that houses the micrometer feed and needle could also be removed and disassembled for cleaning and to replenish the particle supply. A close fit of the top in the acceleration chamber was necessary to maintain alignment of the needle with the system.

A power supply capable of delivering 150 watts at 100 kv provided the accelerating potential. The voltage divider box which supplied the desired voltages and served as a load for the power supply is shown in figure 7. Seven resistors constituted the voltage dividing network; four 10M resistors at the top, two 80M resistors below, and a precision 100K resistor at the bottom. The lead-in from the power supply, at the top right of figure 7 was connected to the needle housing through a protective 500M resistor. The lead from the bolt extending above the top of the acceleration chamber was connected through a 1,000M protective resistor to the juncture of the 10M resistors which provided the desired potential difference between the needle and the thin diaphragm. The voltage across the 100K resistor was proportional to the total accelerating potential and was measured by the electrometer shown in the lower righthand corner of figure 5. Each component resistor was calibrated at operating potentials so that the voltage division ratio and the accelerating potential were known to within ±1%.

The pressure in the acceleration chamber was measured by a Pirani gauge located in the angle valve adjacent to the chamber.

2.2 DIFFERENTIAL PUMPING AND TRACKING CHAMBERS

Two differential pumping chambers were used between the acceleration and tracking chambers. The velocity-measuring chamber, in which particle velocity and charge were determined, was adjacent to the acceleration chamber. The chamber adjacent to the tracking section served only as a differential pumping chamber. The four chambers were connected by three 400-micron orifices.

The velocity measuring section, which was fabricated of aluminum, can be seen in figure 5 directly beneath the acceleration chamber. It is connected to a 7-liter/sec Welch pump through a 2-in.-diameter flexible hose. The pressure was sufficiently low (5 by 10^{-3} torr) so that the particle encountered negligible aerodynamic drag while traversing this section. Therefore, the particle's kinetic energy in this section was exactly equal to the electrical work done in accelerating the particle. The relation expressed by equation 3 is employed to determine the mass of the particle.

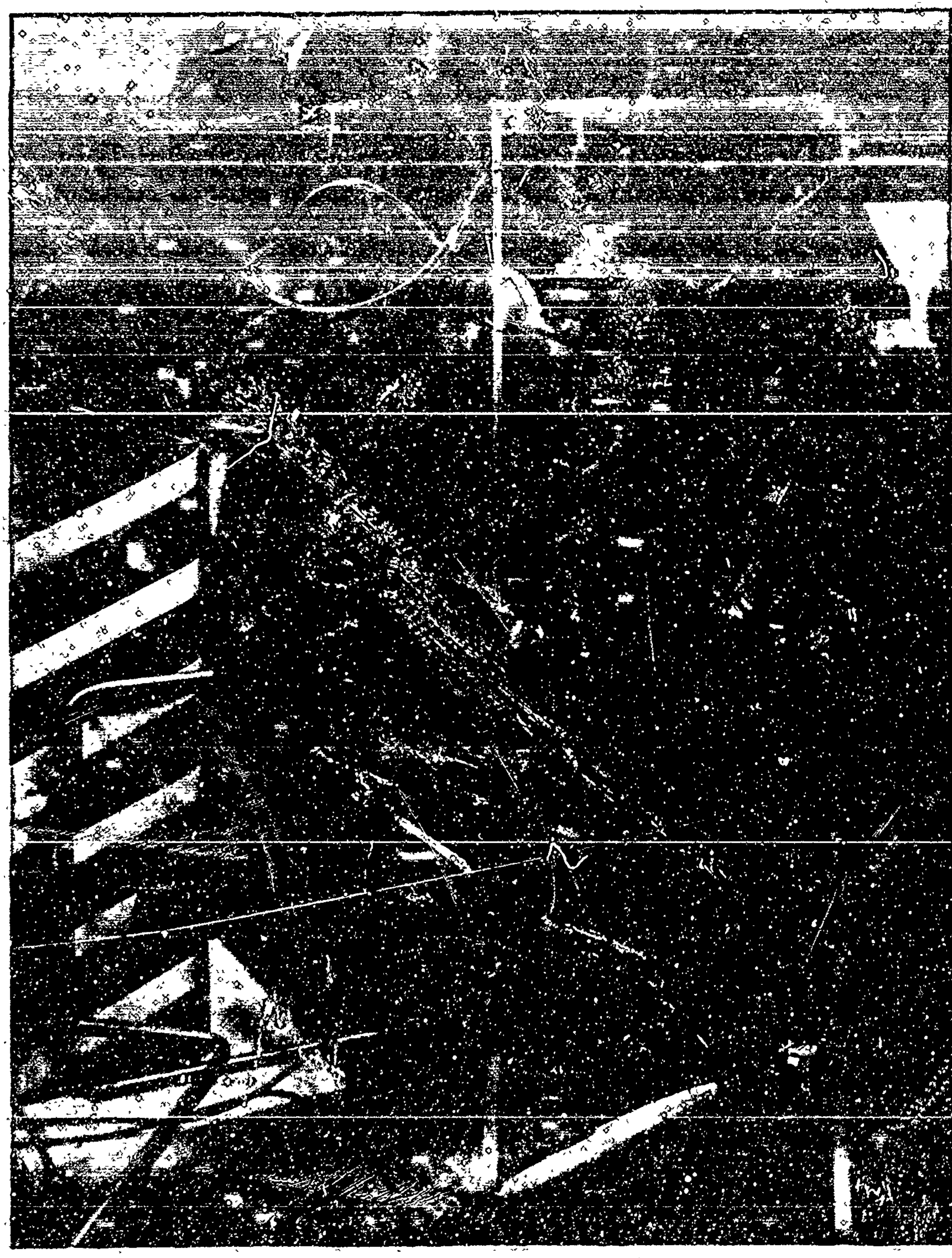

Figure 7. Voltage Divider and Back Side of Experimental Apparatus

90568

The velocity-measuring section was closed on one side by a brass plate which extended the entire length of the differential pumping and tracking sections. The Faraday cage system and cathode-follower amplifiers were mounted on the brass plate which is shown in figure 5. The opposite side of the section was covered by a plate (see figure 7) which supported a Pirani gauge for pressure measurement.

The section adjacent to the tracking chamber was connected to a mechanical vacuum pump through a 1-in.-diameter flexible hose. The two vacuum lines to the differential pumping sections were supported by a massive stand in order to attenuate vibrations from the mechanical vacuum pumps.

The lower section of the apparatus was the tracking chamber. It was enclosed on one side by the brass plate bearing the tracking system and on the opposite side by a plate on which another Pirani gauge, a thermometer, and a pressure tap were mounted (see figure 7). The bulb of the thermometer projected into the chamber to sense the temperature of the gases.

The pressure tap was connected to the manometer (shown in figure 8) on which the tracking-chamber pressure was measured. The two working fluids in the manometer legs were mercury and diffusion pump oil, the latter enabling more precise measurements at lower pressures. The fluid levels were read using the cathetometer.

Gases were fed into the tracking section through the base plate. The flow of gases and, correspondingly, the pressure were controlled by a fine adjustment of a needle valve between the tracking chamber and the gas supply.

System alignment was essential to the successful operation of the experiment. The three 400-micron orifices had to be positioned accurately on a line which extended to the point of the magnetized needle and coincided with the centerline of the Faraday cage system. Each 400-micron orifice was mounted in a larger plug which fitted loosely into 3/8-in. holes between the various sections. This loose fit permitted positioning of the orifice by lateral adjustment screws. Sealing was accomplished through an O-ring face seal. The alignment of the orifices and the needle point was carried out with a light source.

2.3 TRACKING SYSTEM

A series of Faraday cages was the fundamental element of the tracking system. As the charged particle passed through each cage, its charge, or a fraction thereof, was induced on the cage and appeared as a voltage change on the grid of a cathode follower. Thus, as the particle passed each cage, a signal could be observed on an oscilloscope.

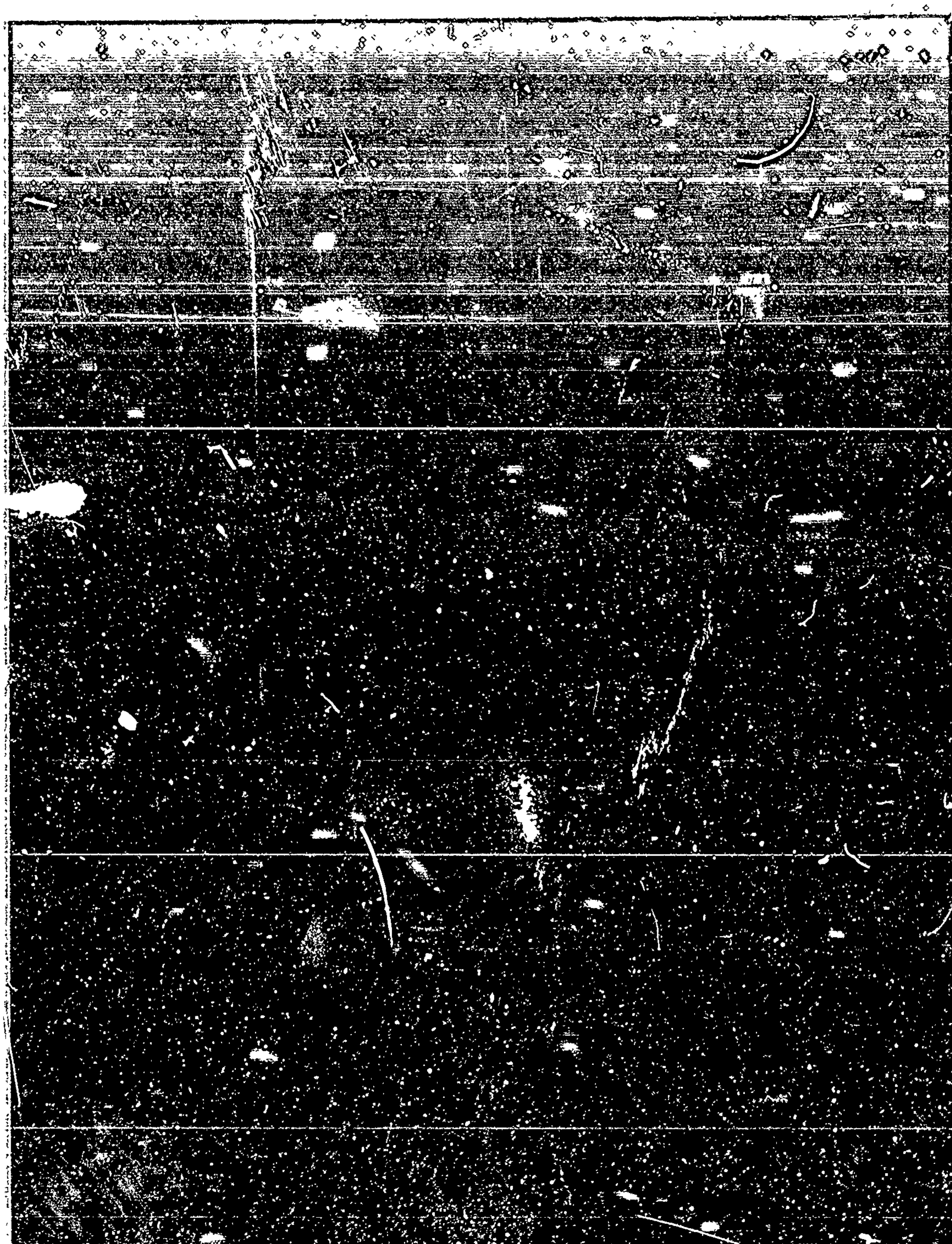

Figure 8. Manometer

90837

The Faraday cages for the velocity-measuring and tracking chambers were mounted on a single plate to facilitate alignment with the system, as shown in figure 9. The series of cages on the left fitted into the velocity-measuring chamber while those to the right comprised the tracking section.

The cages for the velocity-measuring section consisted of a wire stub, three rings, and a tube. The stub, one ring, and the tube are mounted on a wire connected directly to the grid of a miniature high-μ triode (6CW4). The remaining two rings were grounded. The signal generated by the wire stub on passage of a particle served to trigger the oscilloscope.

Eleven rings made up the tracking-section cages. Five of these were connected in common to the grid of another 6CW4, and the other six were grounded. The cages were separated by 1-cm distance in the tracking section and by 1/2-cm in the velocity-measuring section. The distance was measured to within 1/10 of 1% by attaching the system to a machine bed with a fine screw feed and noting when each ring, viewed by a stationary microscope, reached the center of the view field.

A typical oscilloscope trace from the Faraday cage system is shown in figure 10. The scope was triggered by the small wire stub; then the signal went through a minimum as the particle passed the grounded cage. A maximum and a minimum signal were produced as the particle traversed the next signal and grounded cages, and then a longer duration signal was produced as the particle traveled through the tube. The length-diameter ratio of this tube was so large that the particle's entire charge was induced on the tube; therefore, the signal magnitude was directly proportional to the charge on the particle. As the particle proceeded through the tracking section, alternating signal minima and maxima were produced as the particle passed through grounded and signal cages, respectively. The increasing time interval between signal peaks corresponds to the particle deceleration produced by aerodynamic drag.

The question arises as to whether or not the transfer of charge in the Faraday cage system may constitute a decelerative force on the particle. This can be evaluated by comparing the electrical work dissipated to the total change in the kinetic energy of the particle, which is expressed by the ratio

$$\frac{E_{elec}}{E_{KE}} = \frac{i^2 Rt}{\frac{1}{2} m \left(u_o^3 - u_p^2\right)} \tag{4}$$

Figure 9. Faraday Cage Assembly

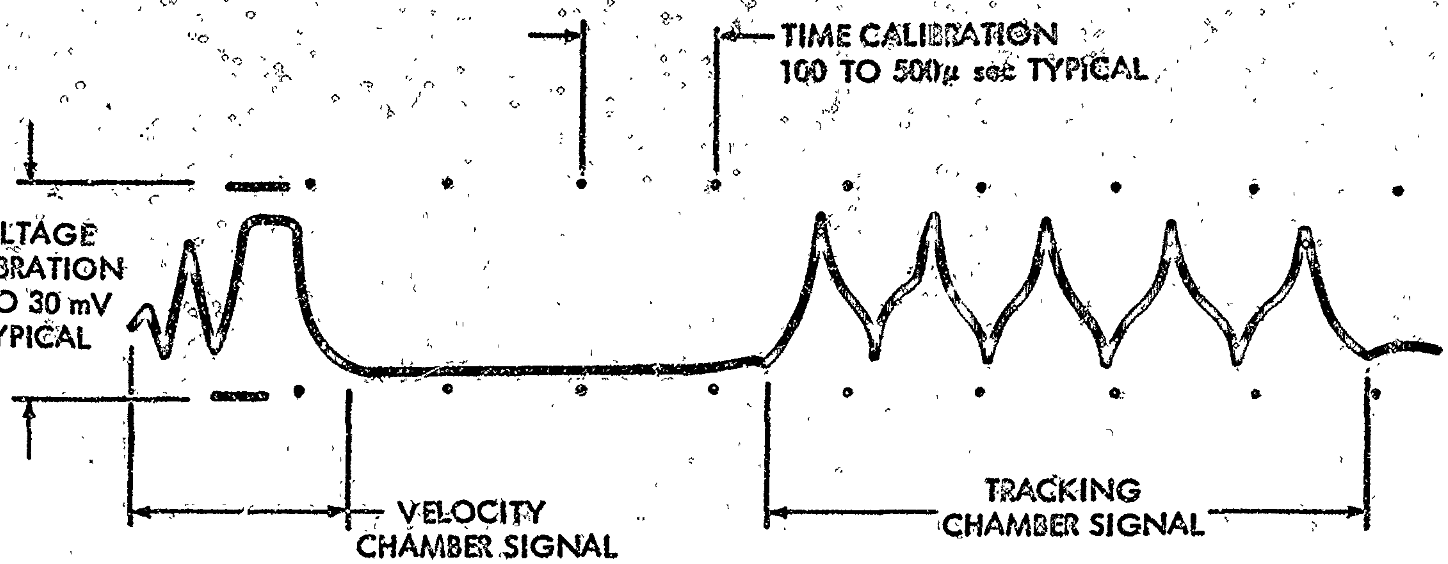

Figure 10. Typical Data Trace from Particle Tracking System

where i is the current, R is the resistance of the Faraday cage system, and t is the time for the particle to pass through the range. The current is estimated by

$$i \simeq \frac{qu_o}{d_c} \tag{5}$$

where d_c is the distance between each cage. Using this approximation and realizing that $u_p/u_o \sim 1$, the above ratio becomes

$$\frac{E_{elec}}{E_{KE}} = \left(\frac{q}{m}\right)^2 \frac{md_R R}{u_o d_c^2 \left(\frac{\Delta u}{u_o}\right)} \tag{6}$$

where d_R is the total range distance. The values of the parameters are

$q/m < 1$ coulombs/kg	$R < 1$ ohm	
$m < 4 \times 10^{-11}$ kg	$u_o > 10$ m/sec	$\frac{\Delta u}{u_o} > 10^{-1}$
$d_R = 10^{-1}$ m	$d_c = 10^{-2}$ m	

which yields

$$\frac{E_{elec}}{E_{KE}} = \mathcal{O}\left(10^{-7}\right) \tag{7}$$

and demonstrates that the effect of the electrical losses on the deceleration of the particle is insignificant.

As discussed above, a high-μ miniature triode is employed in the cathode-follower circuits. The customary grid resistor was omitted, thus allowing a maximum input impedance ($\sim 10^{14}\,\Omega$) and power gain ($\sim 10^{11}$). A low pass filter is inserted in the output to reduce false triggering of the oscilloscope by fast transients originating in other equipment. The voltage gain of the cathode-follower in the velocity-measuring section was measured to be 0.953 to within 1/2 of 1%.

To interpret the voltage signal from the tubular cage in terms of the charge on the particle, it is necessary to know the capacitance of the system. A special capacitance bridge was designed and developed to measure capacitances as low as 4.38×10^{-2} pF. The capacitance of the velocity-section Faraday cage system, positioned in place and under operating conditions, was found to be 6.00 pF to within 1/2 of 1%. Thus, the charge on the particle (q) is related to the voltage signal from the tubular cage (E_s) by

$$q = 5.72\, E_s \times 10^{-12} \pm 1\% \text{ (coulombs)} \tag{8}$$

Two reference signals are put on each oscilloscope trace for measurement purposes. A signal from the internal voltage calibration of the oscilloscope, which was calibrated against a standard cell, provides a reference for measurement of the signal magnitude from the tubular cage. A trace from a time-mark generator (Tektronix 180A) serves to reference the instant of particle passage through each cage. These calibration signals are also shown on figure 10.

3.0 OPERATION OF THE APPARATUS

The aim of the experiment was to obtain drag coefficient data over the entire M-Re regime encountered by particles in a rocket nozzle. The value of M is determined by the particle velocity and the speed of sound in the tracking-section gas. The value of Re is a function of the particle's velocity and size, the pressure in the tracking section, and the working gas.

Each series of experiments was preceded by a thorough cleaning of the acceleration chamber and replenishing of the particle supply. After reassembly the tracking section was flushed and the desired pressure set by a careful adjustment of the needle valve. A period of approximately 30 min was required to stabilize the pressure. The electronic instrumentation was then set and the accelerating potential applied to the system. The micrometer needle was screwed down by a long plastic rod attached to the micrometer handle until the most favorable location was reached and particles of the desired charge and velocity were observed.

The signals from the cathode-followers were fed into a Tektronix 549 storage oscilloscope, and undesirable signals were erased. When a particle of the desired velocity and charge was observed, the oscilloscope intensity was quickly turned down to prevent additional traces from appearing on the screen. An electronic circuit was also developed to translate the base line of each new signal a small amount vertically so that the base lines of several traces could be distinguished.

After selecting and isolating the desired signal, the accelerating voltage, tracking-chamber pressure, and temperature were recorded. Then the voltage and time calibrations were put on the oscilloscope screen. An X-Y plotter, adapted to the oscilloscope, was used to write an identifying number on the screen. Polaroid and 35-mm photographs were then taken of the trace.

Operation of the experiment is illustrated in figure 11. The operator is turning the micrometer drive to feed more particles into the accelerating chamber while prepared, with his left hand, to erase undesired traces.

Usually a series of experiments were conducted at one pressure level by selecting velocities ranging from the smallest to the largest possible. The pressure range was established by the observed velocity decay. If the pressure was too low, insufficient decay occurred for accurate deceleration determination; and if the pressure was too high, the velocity change became

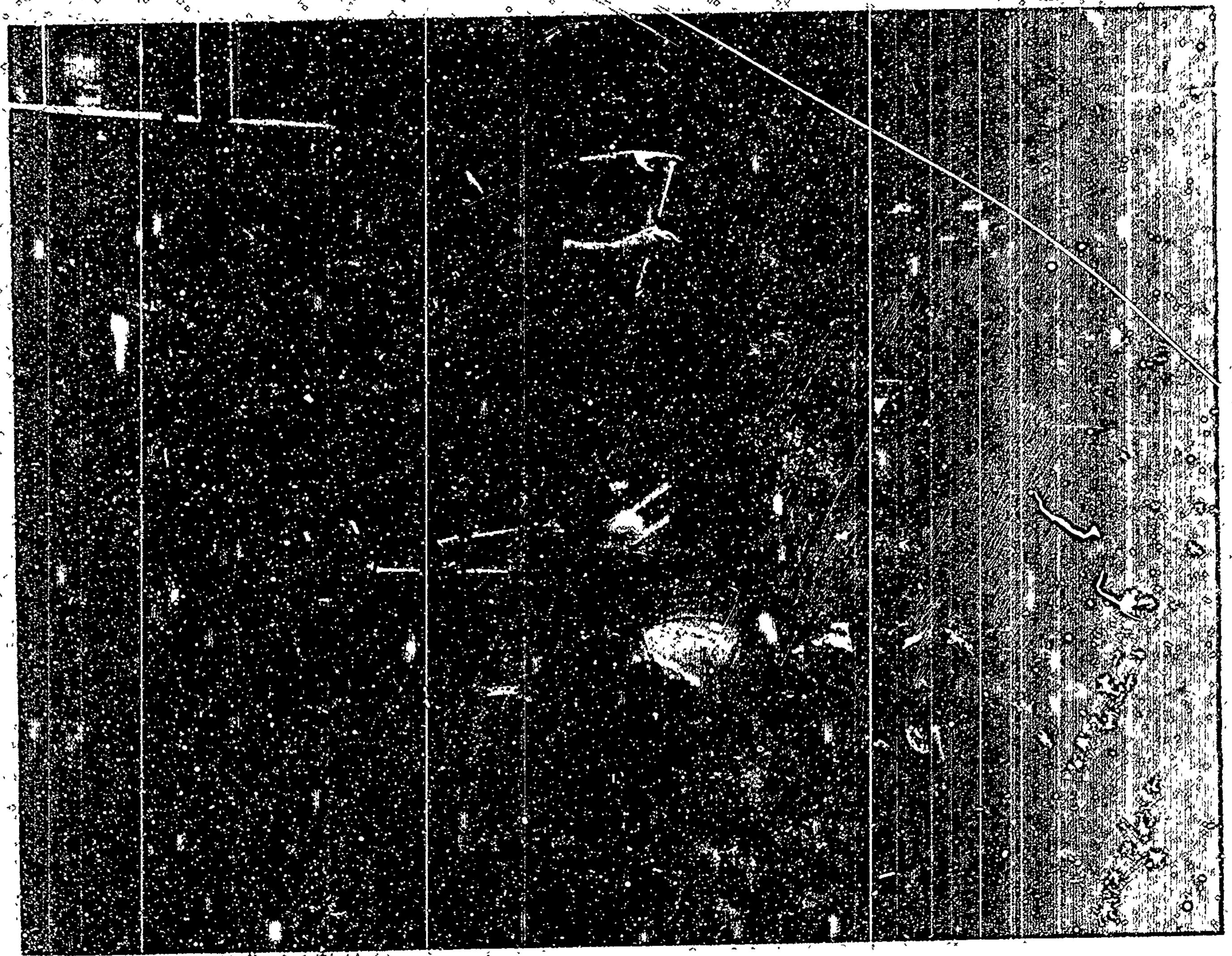

Figure 11. Experimental Operation

90370

too large to represent the test by single values of M and Re. The velocity decays for the data reported here varied between 10% and 40%. After each test the approximate M and Re were plotted to note the relation of each number to the flow regime of interest.

Nitrogen and Freon 114 were employed as working gases. The higher molecular weight of Freon (171 g/mole) corresponds to a lower speed of sound and enabled higher M to be achieved. The pressure in the tracking section was varied between 1 and 50 torr when nitrogen was used and between 1 and 10 torr with Freon.

Two kinds of magnetic particles, carbonyl iron and nickel, were used in the experiments. A scanning electron micrograph of the carbonyl-iron particles is shown in figure 12. It is evident that the particles were not perfect spheres; some appear to have blisters. However the data obtained should still be indicative of the drag coefficients of particles in a rocket nozzle. The nickel particles, on the other hand, were quite spherical as illustrated in figure 13. The size of carbonyl-iron particles measured in the tests ranged from 1.6 microns to 8 microns and the nickel particles from 5 microns to 17 microns in diameter. This agrees reasonably with the sizes observed in the photomicrograph.

The range of M-Re covered by the experiment is illustrated in figure 14. A flow regime which extended from free-molecule flow through transition and just into slip flow was investigated. Thus, the trajectory of a particle in a typical rocket nozzle lies within the range covered.

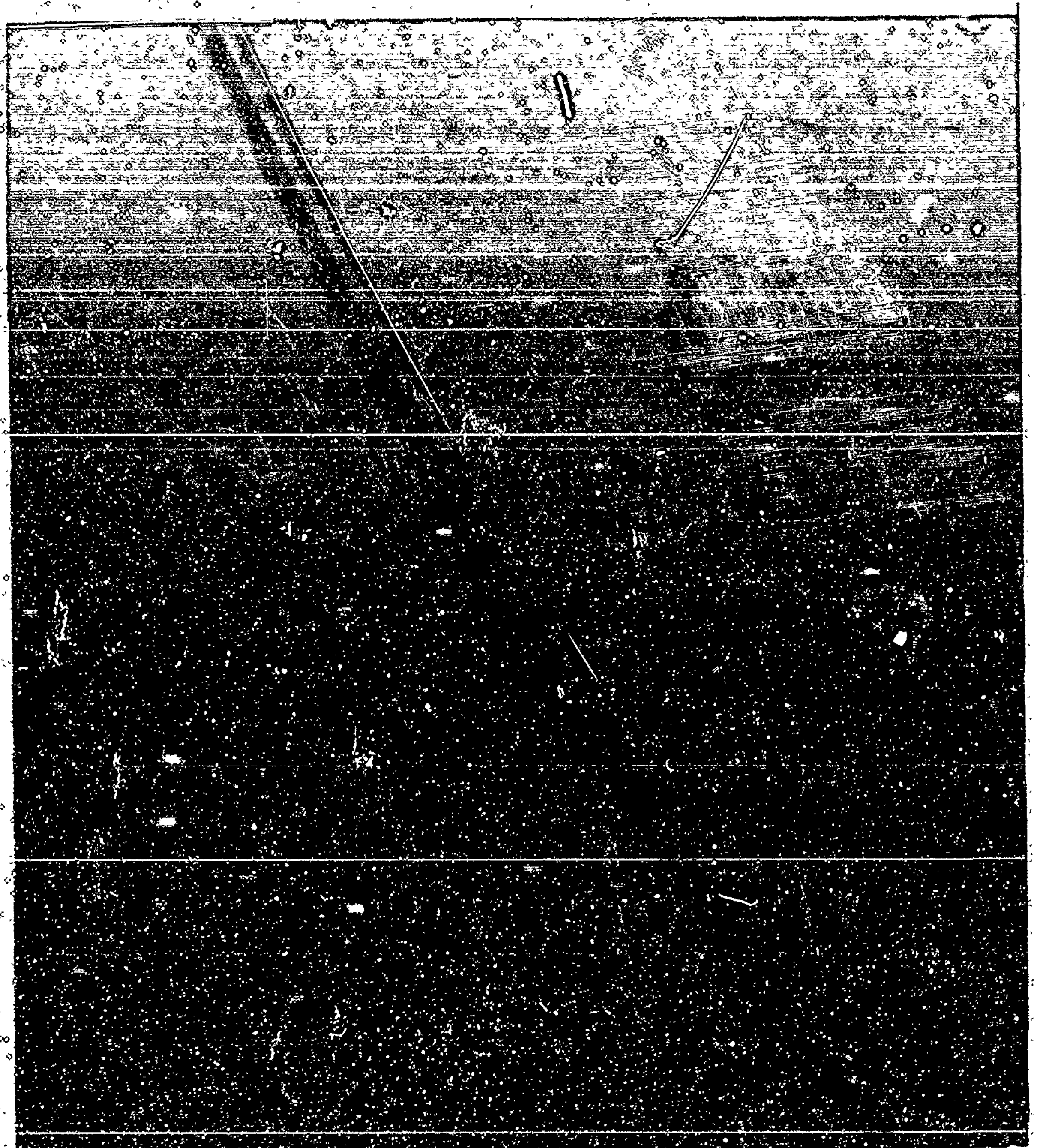

Figure 12. Electron-Microscope Photograph of Carbonyl-Iron Particles

90571

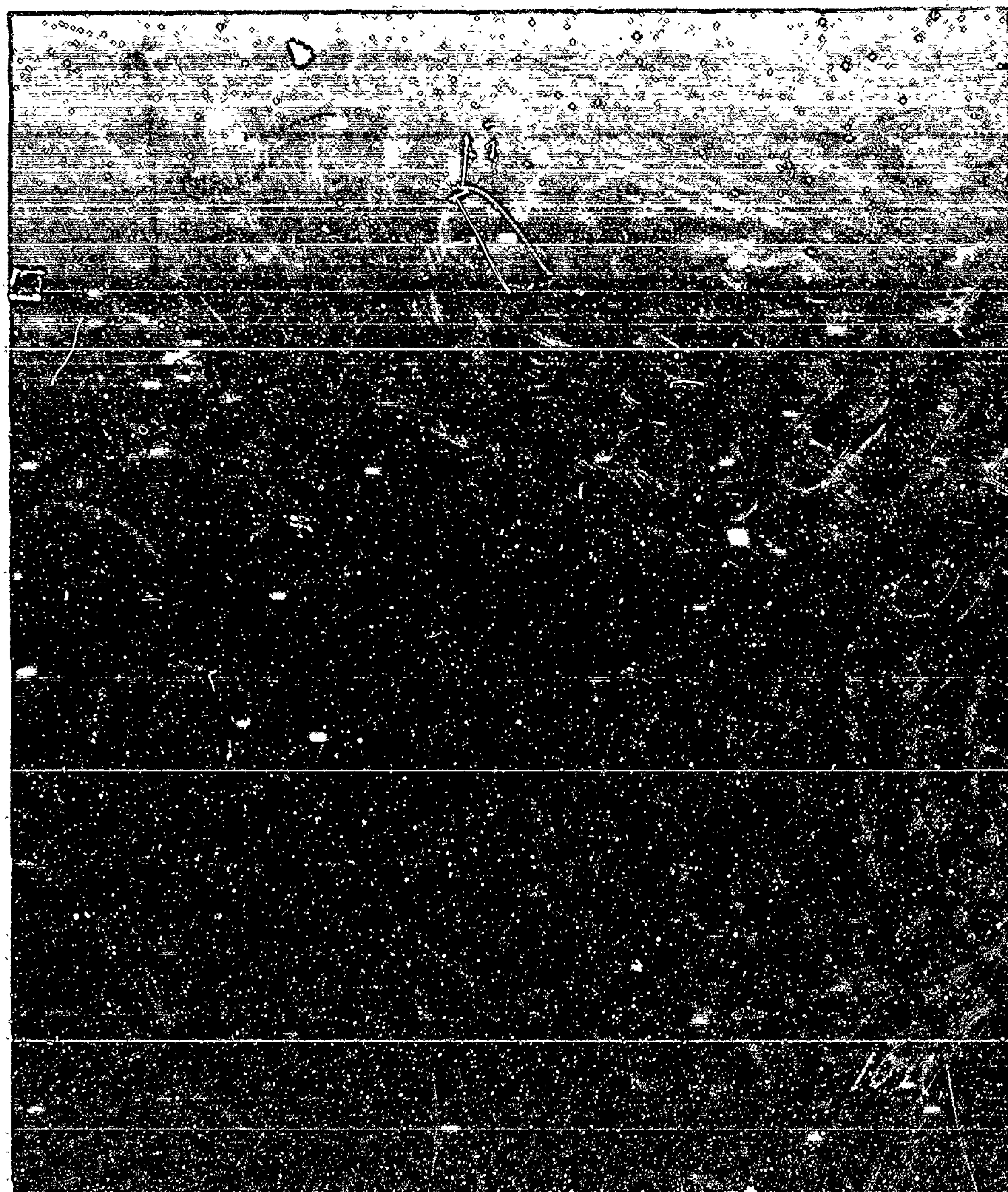

Figure 13. Electron-Microscope Photograph of Nickel Particles

90572

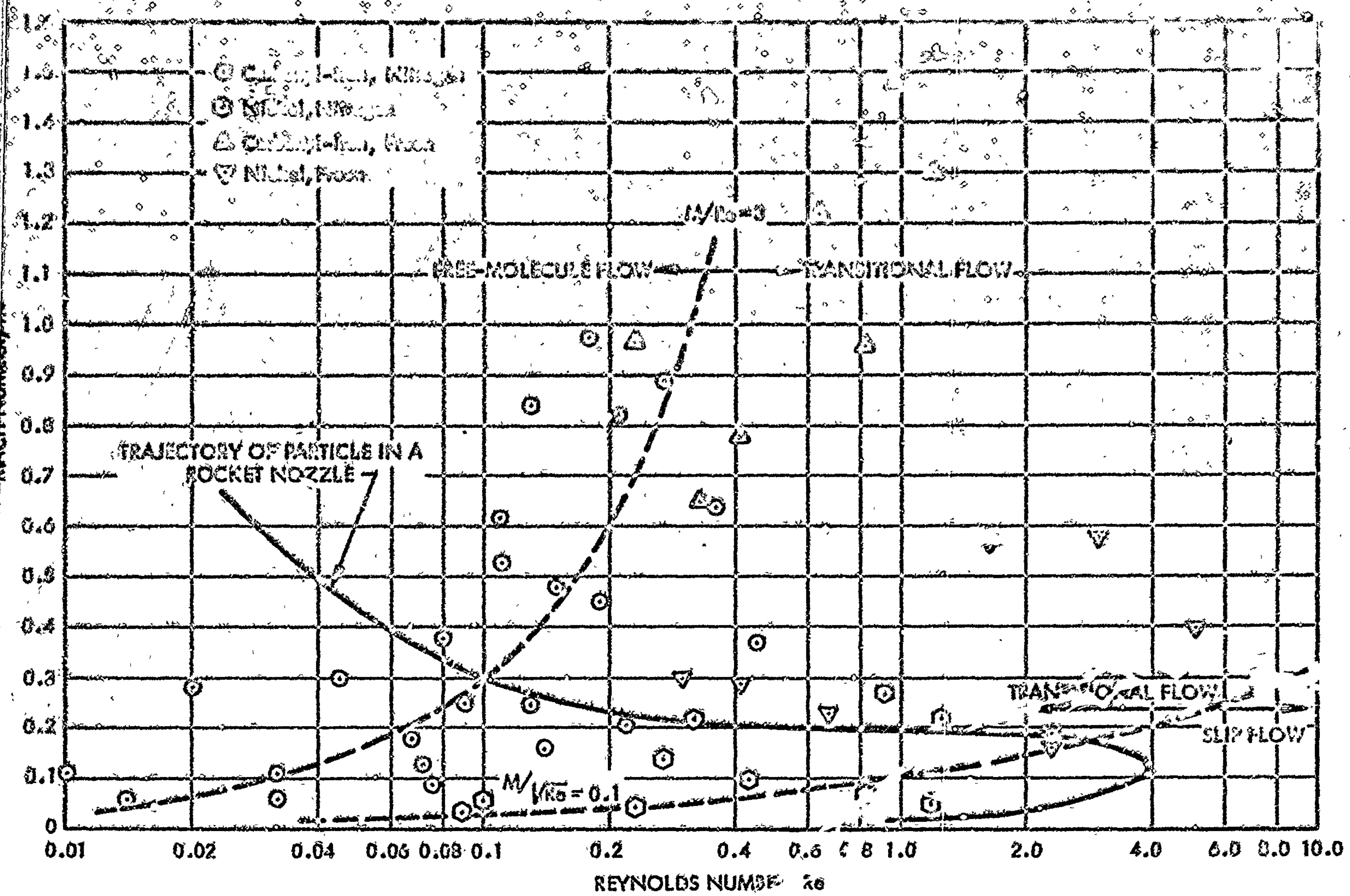

Figure 14. Mach Number-Reynolds Number Regime Covered by the Experiment

53373

4.0 DATA REDUCTION

The fundamental parameters to be reduced from the data were the particle drag coefficient and the corresponding M and Re. The following sections discuss the data reduction technique, its accuracy, and its application to a typical test.

4.1 CALCULATION OF THE DRAG COEFFICIENT FROM DATA

The aerodynamic drag force on a particle is equal to the product of its mass and deceleration. The particle mass is determined when it passes through the velocity-measuring section, and its deceleration is determined from the velocity decay in the tracking section.

Two differentiations of time-distance data to deduce deceleration can lead to significant errors. It is more desirable to use an expression which directly relates drag coefficient and the time-distance data. Equating the aerodynamic drag on a particle and its deceleration yields*

$$m \frac{du_p}{dt} = -C_D \frac{1}{2} \rho_g u_p^2 A \tag{9}$$

Over the range of velocity decay in these experiments, it was reasonable to assume that the drag coefficient was, in essence, constant. The above equation then can be integrated to give the following relation for the time-distance history of the particle

$$t = \frac{1}{u_o} \left(\frac{e^{\alpha s} - 1}{\alpha} \right) + t_o \tag{10}$$

where u_o is the initial velocity of the particle, s the distance traveled in time t, and t_o the time when $s = o$. α is a constant related to the drag coefficient by

$$\alpha = \frac{3}{8} \frac{\rho_g}{\rho_p} \frac{C_D}{r_p} \tag{11}$$

---

*It can be shown that the acceleration due to gravity can be neglected for the range of particle decelerations of these tests.

where ρ_p and r_p are the particle density and radius, respectively. It is convenient to introduce a new variable η where

$$\eta = \frac{e^{\alpha s} - 1}{\alpha} \tag{12}$$

and equation 6 simplifies to

$$t = \frac{1}{u_o} \eta + t_o \tag{13}$$

For a given α, the least-squares technique can be used to determine values of u_o and t_o, corresponding to a straight line on a plot of t versus η, such that

$$E(\alpha) = \sum_{K=1}^{N} \left(t_K - t\right)^2 \tag{14}$$

is a minimum. This was repeated for different values of α to find that value of α for which $E(\alpha)$ is a minimum. (Because the spatial location of each cage was measured to 0.1% there was no need to consider deviations in s.) Having determined the value of α which represented the best fit of the data, the drag coefficient was determined from

$$C_D = \frac{8}{3} \frac{\rho_p}{\rho_g} r_p \alpha \tag{15}$$

A computer program was developed to calculate α for the minimum squared deviation of the data.

An experimental determination of the particle density, using standard analytical techniques, showed that

ρ_p (carbonyl iron) = 7.26 g/cm^3

ρ_p (nickel) = 8.52 g/cm^3

to within 1/10 of 1%.

The gas density was calculated from the temperature and pressure measurements in the tracking chamber, using the equation of state for an ideal gas.

The remaining parameter, r_p, was found from the data obtained by means of the velocity-measuring section. Representing the particles as spheres, one can rewrite equation 3 as

$$r_p = \left(\frac{3}{2\pi}\,\frac{q\,V}{\rho_p\,u_f^2}\right)^{1/3} \tag{16}$$

The measurement of q, V, and the particle velocity, u_f, has been discussed above.

Values of M and Re were calculated using the average particle velocity, i.e., the distance between the first and last tracking cages divided by the transit time.

4.2 ERROR ANALYSIS

The accuracy of the calculated drag coefficient depends on the accuracy with which ρ_p, ρ_g, r_p, and α can be determined. The variance (σ^2) of the drag coefficient is related to that of the independent variables through

$$\frac{\sigma^2_{C_D}}{C_D^2} = \frac{\sigma^2_{\rho_g}}{\rho_g^2} + \frac{\sigma^2_{r_p}}{r_p^2} + \frac{\sigma^2_{\alpha}}{\alpha^2} \tag{17}$$

where the contribution due to ρ_p has been neglected because of the high accuracy with which it was determined. Following standard statistical procedures, the variance, or standard deviation, can be related to the magnitude of error at a chosen confidence level.

The variance of α is determinable from the tracking-section data. It is related to the variance of the time deviation $\left(\sigma^2_{t_K}\right)$ about the least square curve by

$$\sigma^2_{\alpha} = \sum_{K=1}^{N}\left(\frac{\partial\alpha}{\partial\,t_K}\right)^2\sigma^2_{t_K} \tag{18}$$

Assuming the variance is the same for all points yields

$$\sigma_{\alpha}^{2} = \sigma_{t_K}^{2} \sum_{K=1}^{N} \left(\frac{\partial \alpha}{\partial t_K}\right)^2 \tag{19}$$

It can be shown that the sum of the derivatives of α with respect to t_K, subject to the constraint of a minimum sum of squared deviations about the line, is

$$\sum_{K=1}^{N} \left(\frac{\partial \alpha}{\partial t_K}\right)^2 = \frac{N \sum_{K=1}^{N} \eta_K^2 - \left(\sum_{K=1}^{N} \eta_K\right)^2}{\Delta} \tag{20}$$

where

$$\Delta = \frac{1}{u_o^2} \begin{vmatrix} \sum_{K=1}^{N} \left(\frac{\partial \eta_K}{\partial \alpha}\right)^2 & \sum_{K=1}^{N} \eta_K \left(\frac{\partial \eta_K}{\partial \alpha}\right) & \sum_{K=1}^{N} \left(\frac{\partial \eta_K}{\partial \alpha}\right) \\ \sum_{K=1}^{N} \eta_K \left(\frac{\partial \eta_K}{\partial \alpha}\right) & \sum_{K=1}^{N} \eta_K^2 & \sum_{K=1}^{N} \eta_K \\ \sum_{K=1}^{N} \left(\frac{\partial \eta_K}{\partial \alpha}\right) & \sum_{K=1}^{N} \eta_K & N \end{vmatrix}$$

the subscripts K refer to the various distance stations, and N is the number of stations in the tracking section.

The best estimate of the variance of the time deviations is

$$\sigma_{t_K}^{2} = \frac{\sum_{K=1}^{N} \left(t_K - t\right)^2}{N - 3} \tag{21}$$

because of the three degrees of freedom removed by fitting the data with a three-parameter curve. Thus, the variance of α becomes

$$\sigma_\alpha^2 = \frac{\sum_{K=1}^{N}\left(\frac{\partial \alpha}{\partial t_K}\right)^2 \sum_{K=1}^{N}\left(t_K - t\right)^2}{N - 3} \tag{22}$$

The variance of the particle radius, $\sigma_{r_p}^2$, was obtained from

$$\frac{\sigma_{r_p}^2}{r_p^2} = \frac{1}{9}\left[\frac{\sigma_q^2}{q^2} + \frac{\sigma_V^2}{V^2} + \frac{4\sigma_{u_f}^2}{u_f^2}\right] \tag{23}$$

The values of charge q and accelerating potential V were determined from a single reading and, consequently, no information was available on their variance. However absolute errors, ΔV and Δq, were known and were used as upper limits of the variance

$$\sigma_q^2 < (\Delta q)^2$$

$$\sigma_V^2 < (\Delta V)^2$$

The variance of the velocity can be found by fitting the time-distance data in the velocity-measuring section to a straight line and performing the same operations as above for $\sigma_{u_f}^2$. Thus

$$\frac{\sigma_{r_p}^2}{r_p^2} < \left(\frac{\sigma_{r_p}^2}{r_p^2}\right)_{max} = \frac{1}{9}\left\{\left(\frac{\Delta q}{q}\right)^2 + \left(\frac{\Delta V}{V}\right)^2 \cdot 4 \frac{u_f^2 N_v \sum_{K=1}^{N_v} (t_K - t)^2}{(N_v - 2)\left[N_v \sum_{K=1}^{N_v} s_K^2 - \left(\sum_{K=1}^{N_v} s_K\right)^2\right]}\right\} \tag{24}$$

where N_v is the number of stations in the velocity-measuring section. For the data of the present tests it was found that

$$\left(\frac{\sigma_{r_p}}{r_p}\right)^2_{max} << \left(\frac{\sigma_\alpha}{\alpha}\right)^2 \tag{25}$$

and the error in r_p could be neglected.

The variance of the gas density is related to the uncertainty in pressure and temperature measurements by

$$\left(\frac{\sigma_{\rho_g}}{\rho_g}\right)^2 < \left(\frac{\Delta T}{T}\right)^2 + \left(\frac{\Delta P}{P}\right)^2 \tag{26}$$

Once again it was found that this variance is much smaller than $\left(\frac{\sigma_\alpha}{\alpha}\right)^2$ and could be neglected.

Thus, the variance of the drag coefficient becomes simply

$$\left(\frac{\sigma_{C_D}}{C_D}\right)^2 \simeq \left(\frac{\sigma_\alpha}{\alpha}\right)^2 \tag{27}$$

and the error is

$$\left(\frac{\Delta C_D}{C_D}\right) = Q\left(\frac{\sigma_\alpha}{\alpha}\right) \tag{28}$$

where Q was determined from the Student -t distribution for the 75% confidence level.

4.3 REDUCTION OF A DATA POINT FROM A TYPICAL TEST

The trace from a typical test, using carbonyl-iron particles in nitrogen, is shown in figure 15. The small time divisions represent 50 μsec, the larger divisions 0.5 msec intervals. The voltage calibration represents 10 mv. The pressure for this test was measured as 2.24 cm of

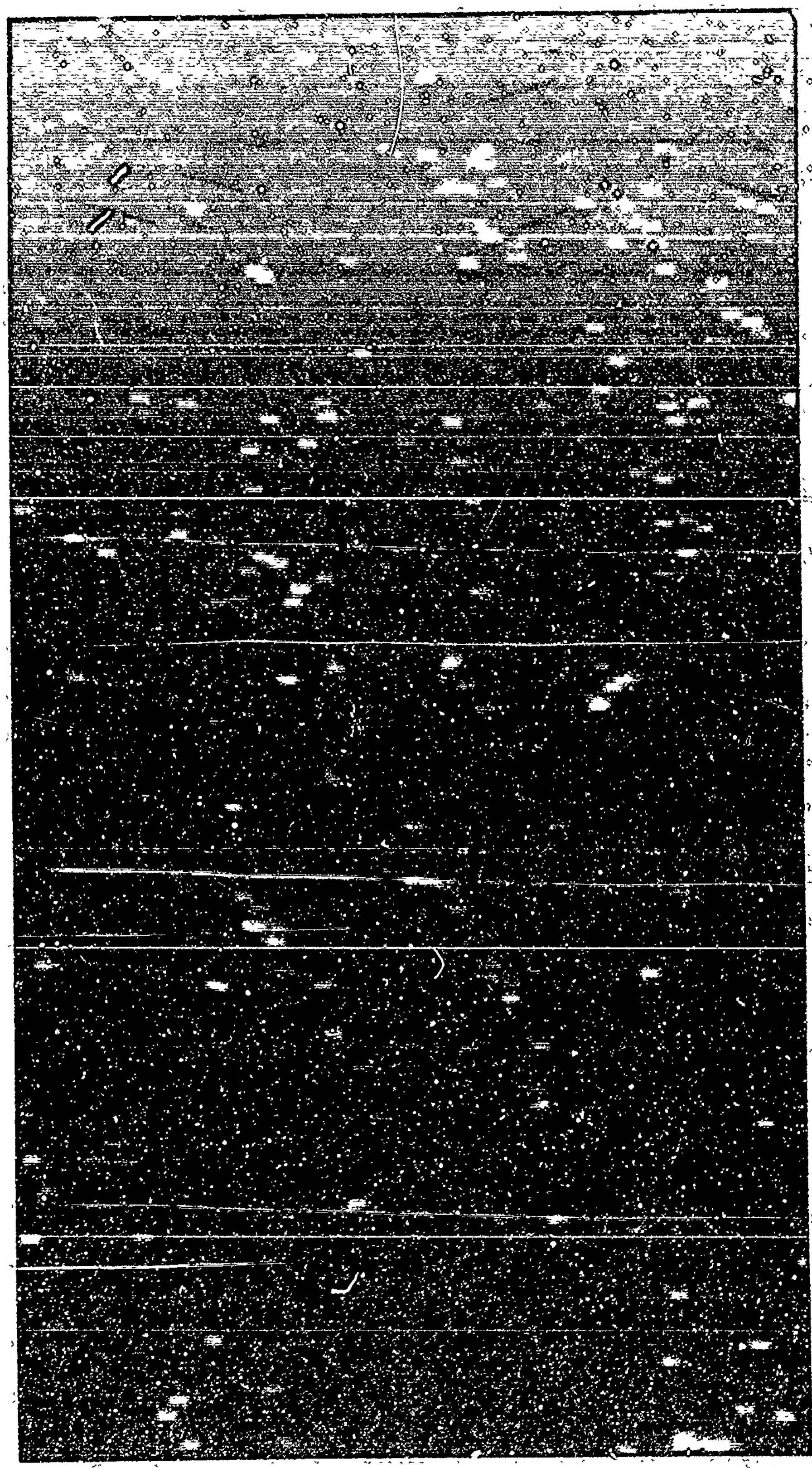

Figure 15. Trace from a Typical Experimental Run

diffusion pump oil, the temperature was 25.5°C, and the potential on the electrometer was 26.0 volts.

The first parameter calculated was the particle radius which was determined from the data of the velocity measuring section. In measuring the distance on the trace between the two grounded cages and relating it to the time calibrations, it is found that the particle traveled 1 cm in 70 μsec or had a velocity of 143 m/sec. Multiplying the electrometer voltage by the calibration factor for the voltage divider, 1.981×10^3, gives an acceleration potential of 51.5 kv. The magnitude of the potential induced on the tubular Faraday cage is measured as 11.35 mv from the trace and the particle charge calculated from equation 4 is $q = 6.5 \times 10^{-14}$ coulombs. Substitution of these data and the density of carbonyl iron into equation 16 yields

$$r_p = 2.2 \text{ microns}$$

The gas density is derived from the pressure and temperature measurements. The density of the diffusion pump oil was measured to be 0.9825 g/cm^3 and, therefore, 2.24 cm of oil is equivalent to 1.62 torr, or 2.16×10^3 dynes/cm^2. This value and a temperature of 25.5°C give

$$\rho_g = 2.44 \times 10^{-6} \text{ g/cm}^3$$

Feeding the time-distance data measured from the tracking-section signal trace into the computer program to determine α and the corresponding error leads to

$$\alpha = 0.00858 \pm 11\%$$

at a 75% confidence level.

Substituting the above values into equation 15 results in

$$C_D = 15.0 \pm 11\%$$

The average velocity in the tracking section was found to have been 134 m/sec which yields

$$Re = 0.081 \quad \text{and} \quad M = 0.38$$

The corresponding Kn is 7.1, and is related to M and Re by [6]

$$Kn = 1.26 \sqrt{\gamma} M/Re \tag{29}$$

After completion of the experiments, it was discovered that a leak had developed in the tracking section and the lower-pressure Freon results were appreciably affected. The magnitude of the leak was determined by comparing nitrogen and Freon data, which overlapped in certain flow regimes, and all the Freon data were corrected accordingly.

A summary of the data is given in table I.

TABLE I

SUMMARY OF EXPERIMENTAL DATA

Test No.	Particle Type and Gas	M	Re	Kn	Particle Drag Coefficient
1	Carbonyl-Iron	0.65	0.36	2.7	7.4±12%
2	Nitrogen	0.88	0.27	4.8	5.5±15%
3		0.97	0.18	8.0	6.3±16%
4		0.25	0.09	4.1	17±13%
5		0.18	0.042	6.4	28±6%
6		0.11	0.032	5.1	52±6%
7		0.061	0.014	6.5	90±22%
8		0.45	0.19	3.5	9.9±14%
9		0.21	0.22	1.4	21±11%
10		0.37	0.45	1.2	11±9%
11		0.16	0.14	1.7	27±14%
12		0.11	0.010	16	61±11%
13		0.18	0.067	3.9	30±10%
14		0.62	0.11	8.4	8.3±7±
15		0.53	0.11	7.2	12±13%
16		0.84	0.13	9.6	7.7±17%
17		0.38	0.080	7.1	15±11%
18		0.30	0.045	9.9	18±16%
19		0.48	0.15	4.8	9.9±11%
20		0.13	0.071	2.7	38±13%
21		0.25	0.13	2.8	21±10%
22		0.82	0.21	5.8	6.8±2%
23		0.092	0.075	1.8	62±12%
24	Carbonyl-Iron	0.060	0.032	2.8	79±9%
25	Nitrogen	0.28	0.020	21.4	21±8%

TABLE I

SUMMARY OF EXPERIMENTAL DATA (Continued)

Test No.	Particle Type and Gas	M	Re	Kn	Particle Drag Coefficient
26	Carbonyl-Iron	0.65	0.33	2.6	8.0±12%
27	Freon	1.48	0.97	2.0	3.7±12%
28		1.77	0.69	3.4	4.0±11%
29		0.97	0.23	5.5	5.8±8%
30		0.78	0.41	2.5	7.8±12%
31		0.96	0.82	1.55	5.3±7%
32	Carbonyl-Iron	1.3	1.20	1.42	4.9±4%
33	Freon	1.22	0.064	26	6.6±18%
34	Nickel	0.048	1.18	0.061	21±10%
35	Nitrogen	0.067	0.82	0.11	30±6%
36		0.22	1.25	0.26	16±4%
37		0.27	0.91	0.44	16±9%
38		0.10	0.43	0.35	31±15%
39		0.036	0.087	0.62	98±13%
40		0.058	0.10	0.86	82±10%
41		0.22	0.32	1.0	25±11%
42	Nickel	0.14	0.27	0.77	29±11%
43	Nitrogen	0.046	0.23	0.30	63±13%
44	Nickel	0.23	0.67	0.48	20±13%
45	Freon	0.29	0.41	0.93	18±10%
46		0.30	0.30	1.32	14±6%
47		0.19	2.3	0.11	9.8±14%
48		0.58	3.0	0.26	6.1±8%
49		0.16	2.3	0.089	11.7±8%
50	Nickel	0.40	5.1	0.10	5.3±10%
51	Freon	0.57	1.63	0.46	8.5±4%

5.0 DATA ANALYSIS

Sherman[7] has shown that drag coefficient data[8, 9, 10] of spheres at high M (M > 4) can be reduced to a nondimensional drag coefficient which depends only on Kn, i. e., the ratio of the mean-free path of the gas molecules to the particle diameter. The nondimensional coefficient is

$$\overline{C_D} = \frac{C_D - C_{D_I}}{C_{D_{FM}} - C_{D_I}} \tag{30}$$

where C_{D_I}* is the drag coefficient for $Re \rightarrow \infty$ and $C_{D_{FM}}$ the free-molecule-flow value.

Ballistic-range data[11] at high Re indicate a constant drag coefficient of 0.92 for M greater than 2. This value was used to C_{D_I} in this M range. However no data are available for the drag coefficient at extremely large Re ($Re > 10^7$) and low M. For purposes of the present analysis, the variation of drag coefficient with M at $Re \sim 10^5$, shown in figure 16, will be used for the C_{D_I} in equation 30.

The drag coefficient of a sphere in free-molecule flow, assuming diffuse reflection of the molecules, is given by

$$C_{D_{FM}} = \frac{\exp(-S^2/2)}{\sqrt{\pi}\, S^3}(1 + 2S^2) + \frac{4S^4 + 4S^2 - 1}{2S^4}\,\mathrm{erf}(S) + \frac{2\sqrt{\pi}}{3S} \tag{31}$$

where S is the speed ratio, which is related to M by

$$S = \sqrt{\frac{\gamma}{2}}\, M \tag{32}$$

*Sherman refers to this parameter as the "inviscid" drag coefficient.

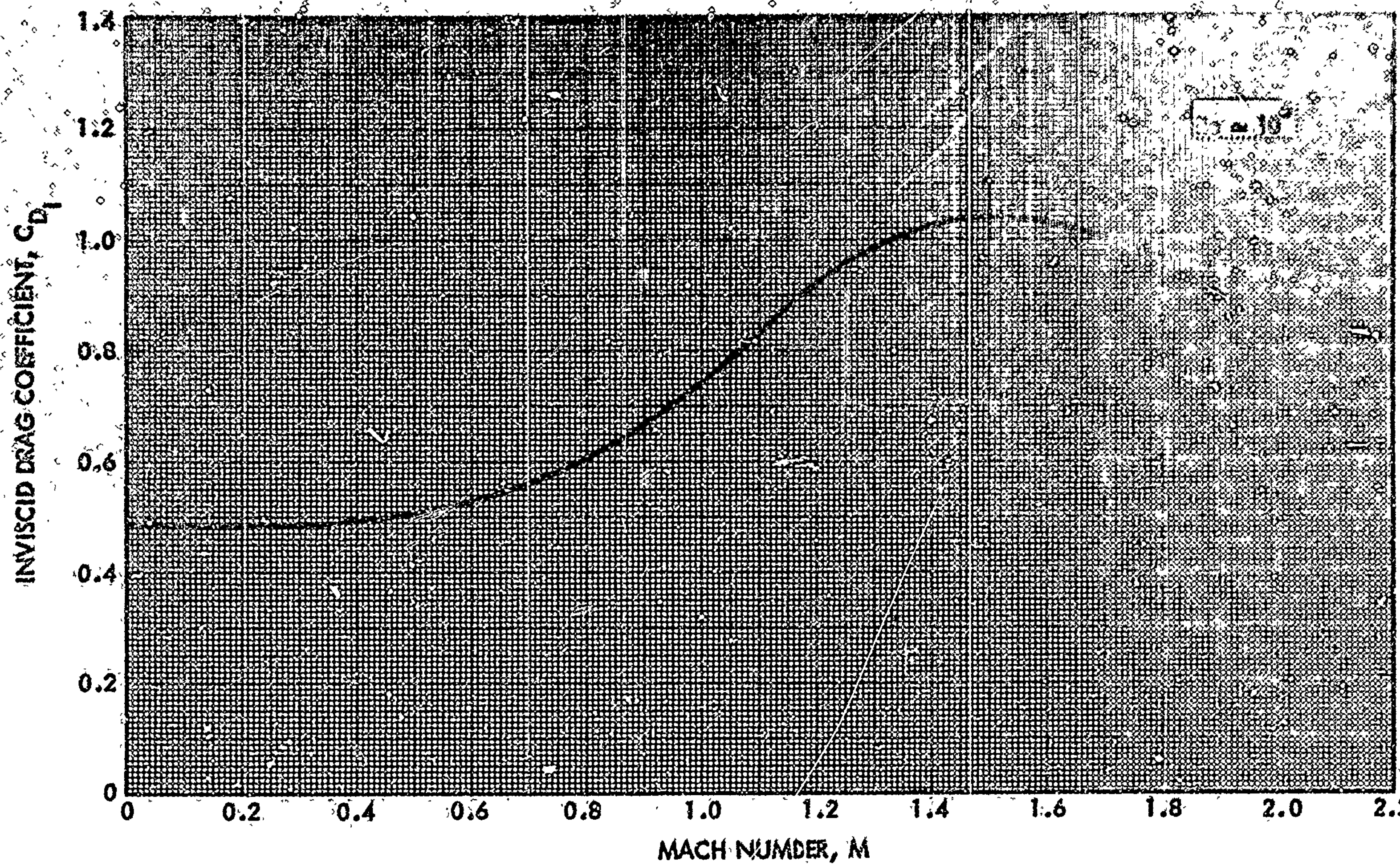

Figure 16. C_{D_I} versus Mach Number

90575

The above equation assumes thermal equilibrium between the particles and the gas. For low M it can be shown that

$$C_{D_{FM}} = \frac{6.3}{\sqrt{\gamma}M} (M << 1) \quad (33)$$

Drag coefficient data obtained in the present experimental studies have been reduced to the nondimensional parameter given by equation 30 and are plotted versus Kn in figure 17. Data from other experiments at high M,[8, 9, 10] Millikan's results[12] from the classical oil drop experiment, and low Re data collected with a magnetic suspension system[13] are shown on the same graph. At high Kn, the data converge to one value, the free molecule-flow limit. Also, for decreasing Kn the data for high M tend to group around a single curve. However, the drag coefficients corresponding to low Re tend to break away from the high M limit with decreasing Kn.

At very low Re in continuum flow where Stokes' law is valid, the drag coefficient is

$$C_D = \frac{24}{Re} \quad (34)$$

Correspondingly, the free-molecule-flow result is given by equation 33 and the nondimensional drag coefficient approaches

$$\overline{C}_D \simeq \frac{24}{6.3} \frac{\sqrt{\gamma} M}{Re} \simeq 3Kn \quad (35)$$

as $Kn \rightarrow 0$. Thus, at low Re, the curve must break away to become asymptotic to the above relation.

Similarly, the necessary asymtote at low Kn for curves at higher Re is

$$\overline{C}_D = Kn\ Re \frac{\left(C_{D_{inc}} - 0.48\right)}{8} \quad (36)$$

where $C_{D_{inc}}$ is the drag coefficient for incompressible flow.

No theoretical analysis is available which provides an analytic expression for the variation of $\overline{C}_D$ with Kn and Re. Some analyses[14, 15] have been published assuming near-free molecule flow, but these are valid only for Kn of unity and greater. A complex Monte-Carlo technique has been developed by Vogenitz, et al.,[16] to treat flows from continuum to free-molecule flow. This technique successfully predicts the measured drag coefficients at high M but does not yield an analytic expression for $\overline{C}_D$ versus Kn.

It is interesting to note that Vogenitz, et. al., predict a drag coefficient at Kn = 100 somewhat higher than the analytic result calculated from the conventional free-molecule-flow analysis. The same tendency is observed in the results of the present study. Millikan's results fall somewhat below the predicted $C_{D_{FM}}$, which is probably attributable to specular reflection from the smooth oil drops.

An empirical expression which reasonably fits the high M data is

$$\overline{C}_{D_{M \gg 1}} = \left[\frac{1.1}{1 + 1.1\,Kn^{-0.3}\exp\left(-Kn^{1/2}\right)}\right] = G(Kn) \qquad (37)$$

and is shown in figure 17. It is assumed that the $\overline{C}_D$ approaches 1.1 as the Kn extends to infinity.

In order to obtain an equation representing all of the data, equation 37 can be multiplied by an empirical factor expressing the break-away of the low Re curves. In the low Kn region, the function G(Kn) is closely represented by

$$G(Kn) \simeq 0.82\,Kn^{0.3} \quad (10^{-3} < Kn < 10^{-1}) \qquad (38)$$

By comparing equations 38 and 36, it is seen that at low Kn the empirical factor must approach

$$Kn^{0.7}\,\frac{\left(C_{D_{inc}} - 0.48\right)Re}{6.6}$$

to give the correct asymptote. A factor incorporating this feature and providing an acceptable fit with the data is

$$L(Kn, Re) = \left\{1 - \exp\left[-Kn\,e^{Kn}\,\frac{\left(C_{D_{inc}} - 0.48\right)Re}{6.6}\right]\right\} \qquad (39)$$

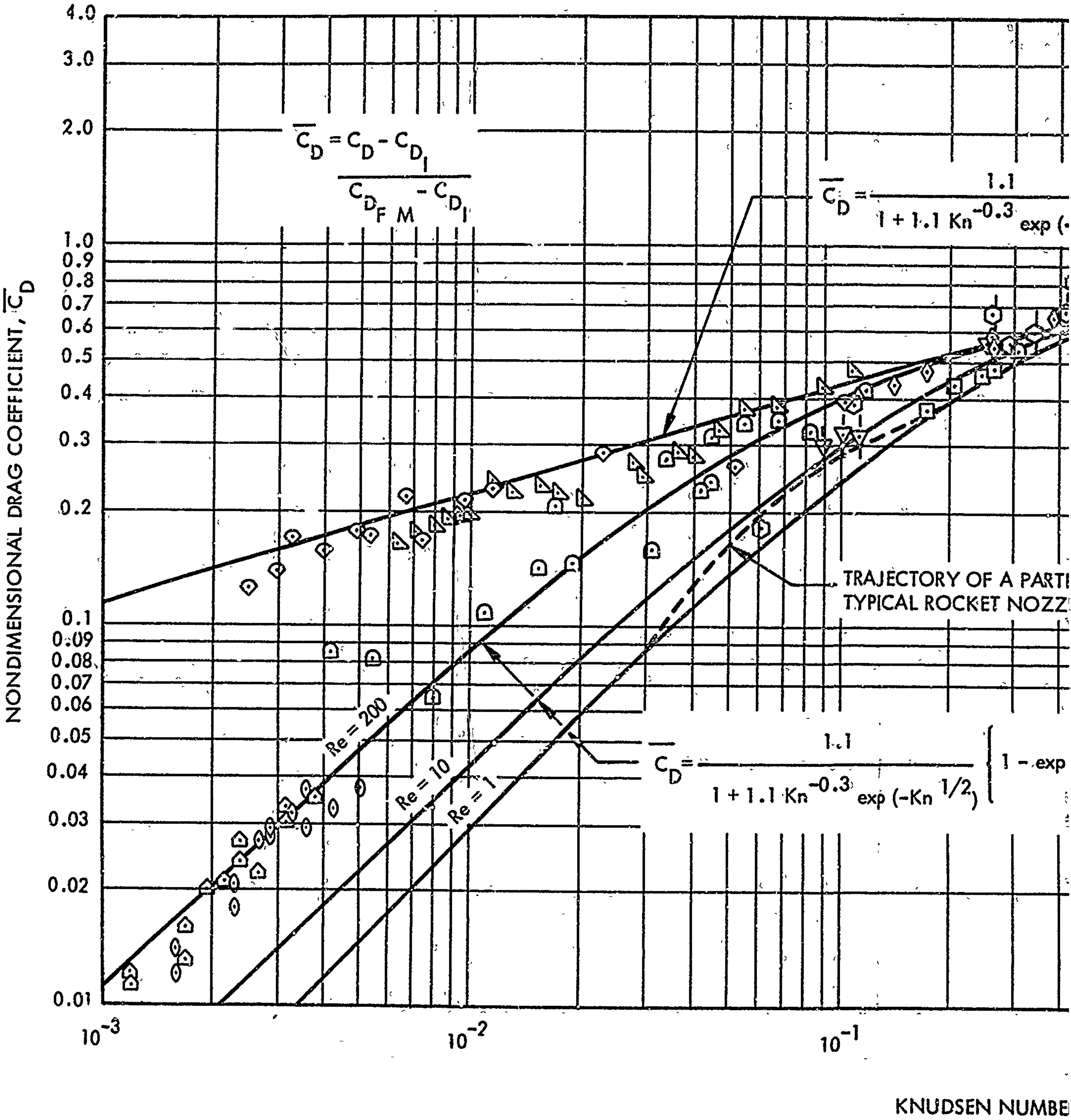

4.0
3.0
2.0
1.0
0.9
0.8
0.7
0.6
0.5
0.4
0.3
0.2
0.1
0.09
0.08
0.07
0.06
0.05
0.04
0.03
0.02
0.01
NONDIMENSIONAL DRAG COEFFICIENT, $\overline{C_D}$
$\overline{C_D} = \frac{C_D - C_{D_I}}{C_{D_{FM}} - C_{D_I}}$
$\overline{C_D} = \frac{1.1}{1 + 1.1\,Kn^{-0.3}\,\exp(\cdot}$
TRAJECTORY OF A PARTI
TYPICAL ROCKET NOZZ
Re = 200
Re = 10
Re = 1
$\overline{C_D} = \frac{1.1}{1 + 1.1\,Kn^{-0.3}\,\exp(-Kn^{1/2})} \left\{ 1 - \exp \right.$
10^{-3}
10^{-2}
10^{-1}
KNUDSEN NUMBE

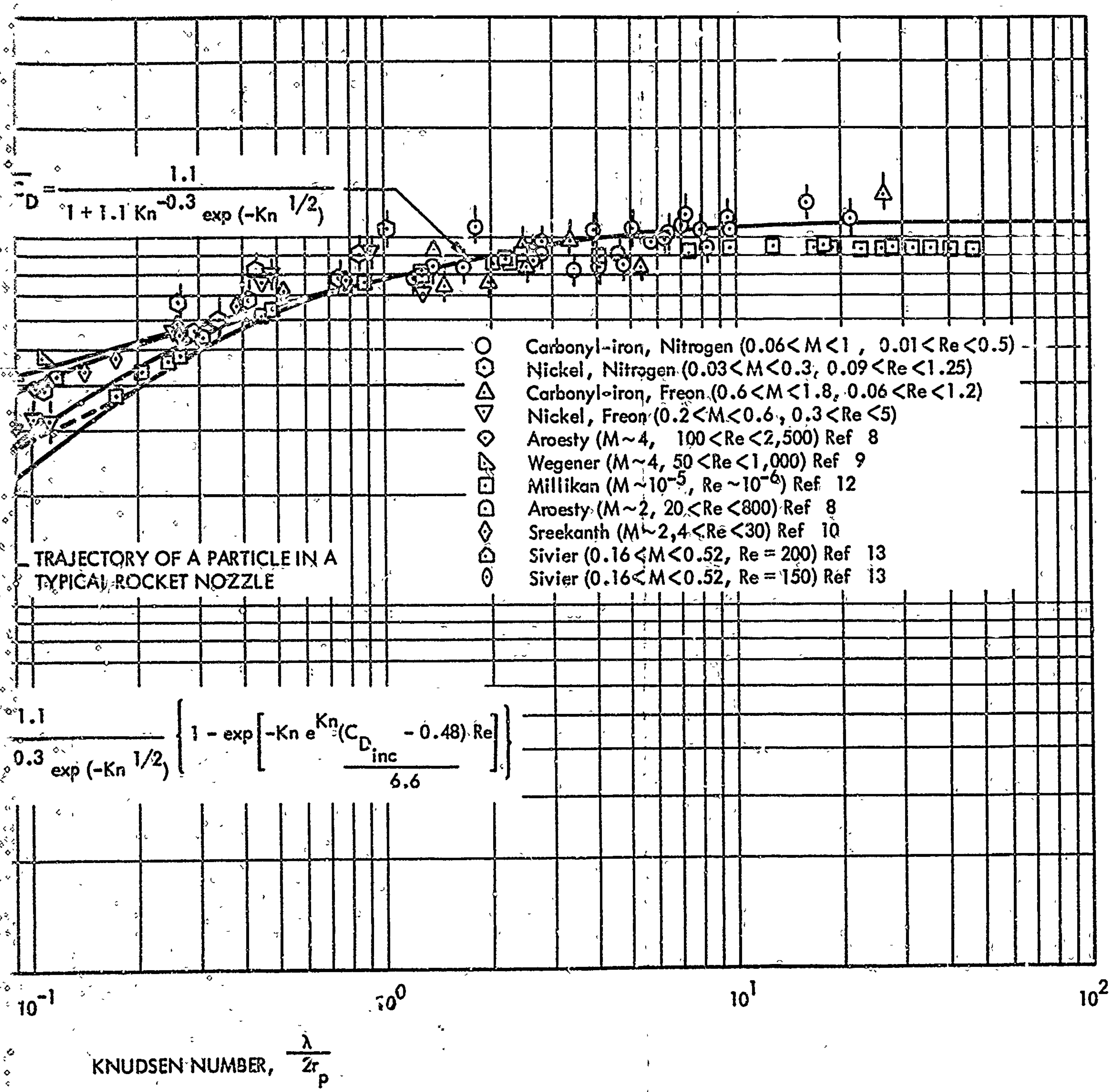

Figure 17. Nondimensional Drag Coefficient for a Sphere vs Knudsen Number

90576

BLANK PAGE

Thus, the complete empirical equation for $\overline{C}_D$ is

$$\overline{C}_D = G(Kn) \cdot D(Kn, Re) \tag{40}$$

Empirical curves for Re = 200, 10, and less than unity, calculated from equation 40, are shown in figure 17. Agreement with the available data is good and equation 40 is recommended for calculating the drag coefficients of particles in a rocket nozzle.

It is enlightening to trace the trajectory of a particle in a rocket nozzle with reference to figure 17. The Kn of a particle is given by

$$Kn = 1.26 \frac{\sqrt{\gamma}\,\mu_g}{2r_p \, \rho_g \, a} \tag{41}$$

where μ_g is the gas viscosity and a the local speed of sound. Because the gas density decreases monotonically with distance through the nozzle, the Kn monotonically increases. The Kn of a 3-micron particle in a 200-psi rocket chamber is 0.031. Thus, the trajectory begins on the $Re < 1$ line at the chamber Kn, goes through the maximum Re in the throat region where $Kn \sim 0.06$, and proceeds back toward the $Re < 1$ curve with increasing Kn, traversing the whole flow regime covered by this study.

It is interesting to compare the data with expressions devised for drag coefficient versus M and Re before the data were available. Crowe[2] proposed

$$C_D = \left(C_{D_{inc}} - 2\right) \exp\left[-3.07\sqrt{\gamma}\,\frac{M}{Re}\,g\,(Re)\right] + \frac{h(M)}{\gamma^{1/2}\,M}\,e^{-\frac{Re}{2M}} + 2 \tag{42}$$

where $\log_{10} g\,(Re) = 1.25\left[1 + \tanh\,(0.77 \log_{10} Re - 1.92)\right]$

and

$$h(M) = \left[2.3 + 1.7\,(T_p/T_g)^{1/2}\right] - 2.3 \tanh\,(1.17 \log_{10} M)$$

T_p/T_g is the particle temperature – gas temperature ratio which, for this comparison, is unity. Carlson[17] suggested the formula

$$\frac{C_D\,Re}{24} = \frac{(1 + 0.15\,Re^{0.687})\left[1 + \exp(-0.427/M^{4.63})\,\exp(-3/Re^{0.88})\right]}{1 + \frac{M}{Re}\left[3.82 + 1.28\,\exp(-1.25\,Re/M)\right]} \tag{43}$$

based on various analytic and empirical trends. Kliegel[18], in his two-phase flow analysis, has used the drag coefficient predicted by solving the 13 moment equations for flow over a sphere, namely

$$C_D = C_{D_{inc}}\left[\frac{(1 + 7.5\,Kn)(1 + 2\,Kn) + 1.91\,Kn^2}{(1 + 7.5\,Kn)(1 + 3\,Kn) + (2.29 + 5.16\,Kn)\,Kn^2}\right] \tag{44}$$

The above three expressions for drag coefficient are plotted on figure 18. The various data are also shown for reference. All the curves correspond to an Re of unity. It is noted that all the curves become parallel with the asymptotic line for Stokes flow at low Kn ($\overline{C}_D \simeq 3$ Kn), but are somewhat higher because the drag coefficient at Re = 1 is slightly larger than predicted by Stokes drag law. With increasing Kn, the drag coefficient expressions used by Carlson and Kliegel diverge significantly from the data. The expression proposed by Crowe shows better agreement but displays an undesirable inflection in the near-free-molecule flow regime, near Kn = 6. Such an inflection is not predicted by present theories, and the use of equation 42 is not recommended.

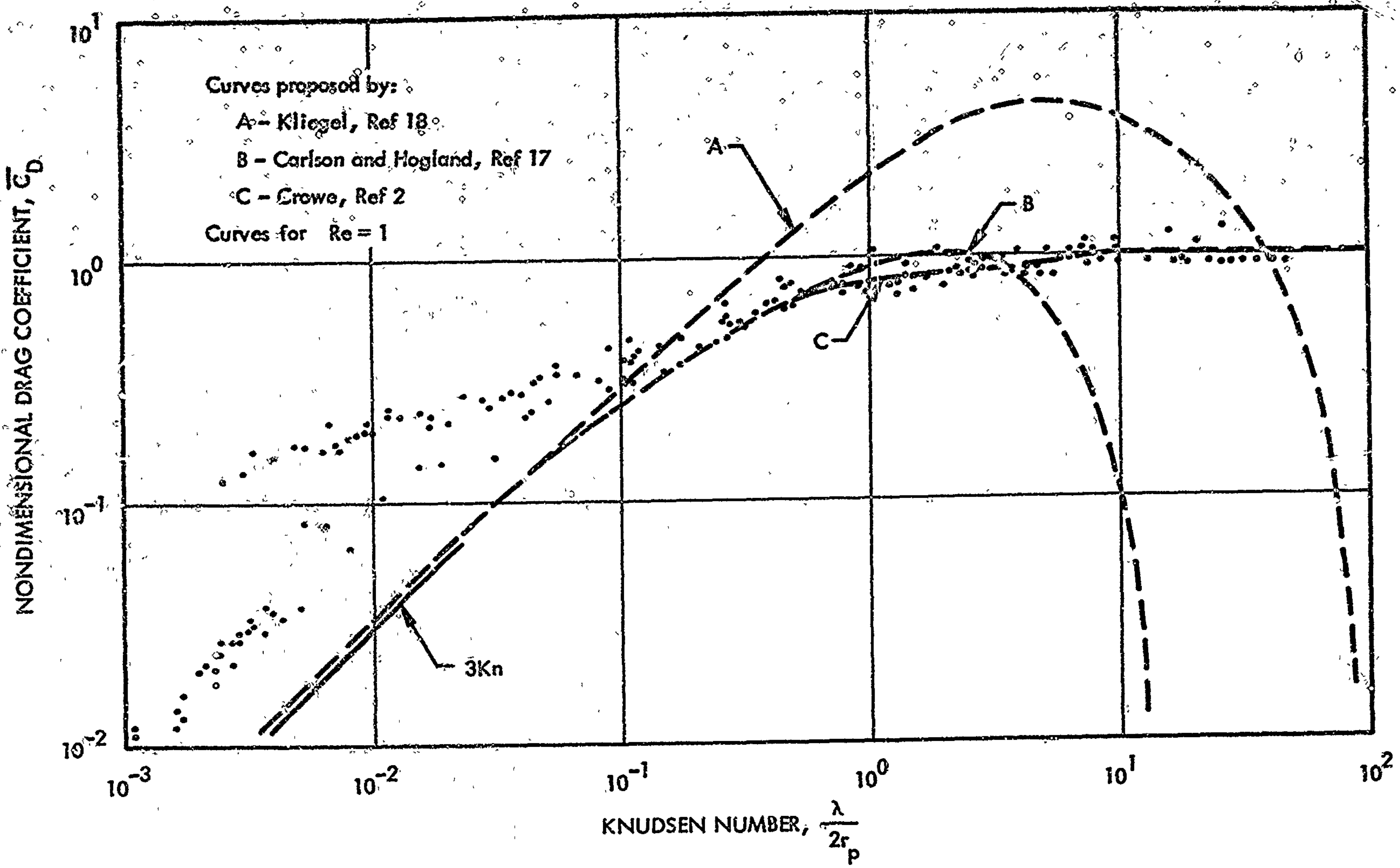

Figure 18. Comparison of Proposed Expressions for Particle Drag Coefficient

20577

6.0 CONCLUSION

Drag coefficients for spherical particles were measured over a range of M and Re corresponding to flow regimes encountered by particles in a rocket nozzle. The data were reduced in terms of a nondimensional drag coefficient and correlated, together with available data obtained under other flow conditions, in terms of two fundamental parameters: Re and Kn. An empirical equation, valid for all Re and for Kn from 0.001 to infinity, was developed for the nondimensional drag coefficient. This equation is recommended for use in calculations of gas-particle flow in rocket nozzles.

7.0 LITERATURE CITED

1) "Dynamics of Two-Phase Flow in Rocket Nozzles," UTC 2102-FR, Contract No. NOW-64-0506-c. United Technology Center, [illegible] September 1965.

2) Crowe, C. T., "Drag Coefficient of Particles in a Rocket Nozzle," AIAA Journal, 5, p. 1022, 1967.

3) Palmer, E. P., D. R. Harrison, and R. W. Grow, "Charging, Initial Acceleration and Detection of Micron Diameter Particles," TR No. 65R-2[illegible] University of Utah, 5 December 1961.

4) Shelton, H., C. D. Hendricks, Jr., and R. F. Wuerker, "Electrostatic Acceleration of Microparticles to Hypervelocities", Journal of Applied Physics, 31, 7, pp. 1243–1246, July, 1960.

5) Alpert, D., et. al., "Initiation of Electrical Breakdown in Ultrahigh Vacuum," The Journal of Vacuum Science and Technology, I, p. 35, 1964.

6) "Fundamentals of Gas Dynamics," High Speed Aerodynamics and Jet Propulsion, Vol 3, edited by H. W. Emmons. Princeton University Press.

7) Sherman, F. S., "A Survey of Experimental Results and Methods for The Transition Regime of Rarefied Gas Dynamics," Rarefied Gas Dynamics, Vol 2, Supplement 2, pp. 228–259, 1963.

8) Aroesty, J. "Sphere Drag in a Low-Density Supersonic Flow," TR HE-150-192, University of California, Institute of Engineering Research, 1962.

9) Wegener, P. P., and H. Ashkenas, "Wind Tunnel Measurements of Sphere Drag at Supersonic Speeds and Low Reynolds Numbers," JPL Tech. Release No. 34-160, NASA Contract No. NASW-6, Nov. 1960.

10) Sreekanth, A. K., "Drag Measurements on Circular Cylinders and Spheres in the Transition Regime at a Mach Number of Two," UTIA Report 74. University of Toronto, 1961.

11) May, A., and W. R. Witt, "Free Flight Determinations of the Drag Coefficients of Spheres," Journal of the Aeronautical Sciences, 20, pp. 635–638, 1953.

12) Millikan, R. A., "The General Law of Fall of a Small Spherical Body Through a Gas, and its Bearing upon the Nature of Molecular Reflection from Surfaces," The Physical Review, 22, p. 1, 1923.

13) Sivier, K. R., "Subsonic Sphere Drag Measurements at Intermediate Reynolds Numbers," Ph.D. Thesis, University of Michigan, 1967.

14) Rose, M. H., "Drag on an Object in Nearly Free Molecular Flow," Physics of Fluids, 7, pp. 1262–1269, 1964.

15) Baker, R., and A. Charwat, "Transitional Correction to the Drag on a Sphere in Free Molecule Flow," Physics of Fluids, 1, 73, 1958.

16) Vogenitz, F. W., et. al., "Theoretical and Experimental Study of Low Density Supersonic Flows about Several Simple Shapes," AIAA paper 68-6, Sixth Aerospace Sciences Meeting, New York, 22 through 24 January 1968.

17) Carlson, D. J., and R. F. Hogland, "Particle Drag and Heat Transfer in Rocket Nozzles," AIAA Journal 2, pp. 1980–1984, 1964.

18) Kliegel, J. R., "Gas Particle Nozzle Flows," Ninth International Symposium on Combustion, Academic Press, pp. 811–827, 1963.

8.0 PARTICIPATING PERSONNEL

The professional personnel who actively participated in this project were C. [illegible], W. Babcock, P. Willoughby, R. Carlson, and R. W. [illegible].

UNCLASSIFIED
Security Classification

DOCUMENT CONTROL DATA - R & D

(Security classification of title, body of abstract and indexing annotation must be entered when the overall report is classified)

1. ORIGINATING ACTIVITY (Corporate author) United Technology Center P. O. Box 358 Sunnyvale, California 94088	2a. REPORT SECURITY CLASSIFICATION Unclassified 2b. GROUP

3. REPORT TITLE

Measurement of Particle Drag Coefficients in Flow Regimes Encountered by Particles in a Rocket Nozzle

4. DESCRIPTIVE NOTES (Type of report and inclusive dates)

Final Report covering the period 1 September 1967 through 28 February 1969

5. AUTHOR(S) (First name, middle initial, last name)

Clayton T. Crowe, Wayne R. Babcock, Paul G. Willoughby, and Robert L. Carlson

6. REPORT DATE	7a. TOTAL NO. OF PAGES	7b. NO. OF REFS
31 March 1968	48	18

8a. CONTRACT OR GRANT NO. Contract No. DAH-C04-67-C-0057 b. PROJECT NO. Project 6656-E c. d.	9a. ORIGINATOR'S REPORT NUMBER(S) UTC 2296-FR 9b. OTHER REPORT NO(S) (Any other numbers that may be assigned this report)

10. DISTRIBUTION STATEMENT

This document is subject to special export controls, and each transmittal to foreign governments or foreign nationals may be made only with prior approval of U.S. Army Research Office.

11. SUPPLEMENTARY NOTES	12. SPONSORING MILITARY ACTIVITY U.S. Army Research Office Durham, North Carolina

13. ABSTRACT

Under contract to the Army Research Office, United Technology Center has conducted an experimental investigation to determine the drag coefficient of particles in flow regimes encountered in a rocket nozzle. The acquisition of these data leads to more reliable predictions of nozzle performance inefficiencies owing to gas-particle flow.

The Mach number-Reynolds number regime traversed by a particle in a rocket nozzle is described. The experiment to determine drag coefficient data in this flow regime consists of the electrostatic acceleration of micron-size particles to sonic velocities and detection of their velocity decay in a chamber conditioned to provide the desired flow parameters. The operation of the experiment, method of data reduction and analysis of the experimental error are presented.

The data are reduced in terms of a nondimensional drag coefficient and correlated with comparable data obtained in other flow regimes. An empirical relation is generated for the drag coefficient as a function of Reynolds and Knudsen numbers. This relation is recommended for use in calculations of gas-particle flow in rocket nozzles.

DD FORM 1 NOV 65 1473

UNCLASSIFIED
Security Classification